REPORT 1317

CLOUD-DROPLET INGESTION IN ENGINE INLETS WITH INLET VELOCITY RATIOS OF 1.0 AND 0.7[1]

By RINALDO J. BRUN

SUMMARY

The paths of cloud droplets into two engine inlets have been calculated for a wide range of meteorological and flight conditions. The amount of water in droplet form ingested by the inlets and the amount and distribution of water impinging on the inlet walls are obtained from these droplet-trajectory calculations. In both types of inlet, a prolate ellipsoid of revolution represents either part or all of the forebody at the center of an annular inlet to an engine. The configurations can also represent a fuselage of an airplane with side ram-scoop inlets. The studies were made at an angle of attack of 0°. The principal difference between the two inlets studied is that the inlet-air velocity of one is 0.7 that of the other. The studies of the two velocity ratios lead to some important general concepts of water ingestion in inlets.

INTRODUCTION

As part of a comprehensive program on cloud-droplet-trajectory computations, the NACA Lewis laboratory has calculated the paths of droplets ahead of and surrounding prolate ellipsoids of revolution moving through clouds (refs. 1 to 4). The present report extends the trajectory computations with respect to prolate ellipsoids in an incompressible flow field to include the study of water ingestion in two engine inlets at 0° angle of attack. In both inlets, an ellipsoid represents either part or all of the forebody at the center of an annular inlet to an engine, or some other air-processing device. In either inlet, the ellipsoid can also be assumed to approximate the fuselage of an airplane so that the inlets become side ram-scoop inlets.

The configurations, which are described in detail in the following section, are geometrically simple in order to permit the studies described herein. In spite of the simplicity, the configurations are reasonable approximations of those found on aircraft. The results of the studies on the two simple shapes lead to important general concepts of water ingestion into inlets of this type.

DESCRIPTION OF CONFIGURATIONS

In order to make a study of impingement on inlets, it is necessary to devise a model configuration for which the airflow field can be obtained and which reasonably represents an actual inlet on an airplane. The models chosen for this study are basically dependent on the air velocity flow field surrounding a prolate ellipsoid of revolution. Both inlet configurations consist of an annulus surrounding an ellipsoid of revolution as the forebody.

The inlets differ somewhat in physical appearance as well as in the entrance velocity of the air. In one inlet configuration, the cowl, or outer wall, is infinitely thin and conforms to the shape of an air streamline. With this inlet there are many possible locations of the outer wall with respect to the ellipsoid forebody. A possible configuration is shown in figure 1(a). The cowl of the other inlet configuration has a slight thickness, as shown in figure 1(b). This outer wall has a fixed configuration with respect to the ellipsoid forebody $\overline{AB}$. The inner surface of the cowl and the inlet inner wall are straight and parallel. Either of the inlets shown in figure 1 may be a complete annulus surrounding the forebody or a sector of an annulus such as would be found in side ram-scoop inlets.

The ellipsoids chosen for this study are 10 and 20 percent thick (fineness ratios of 10 and 5, respectively) for configuration 1 (fig. 1(a)) and 10 percent thick for configuration 2 (fig. 1(b)). The problem is limited to an angle of attack of 0° between the major axis of the ellipsoid and the free-stream air, because the facile methods of calculating the flow field and trajectories are limited to 0°.
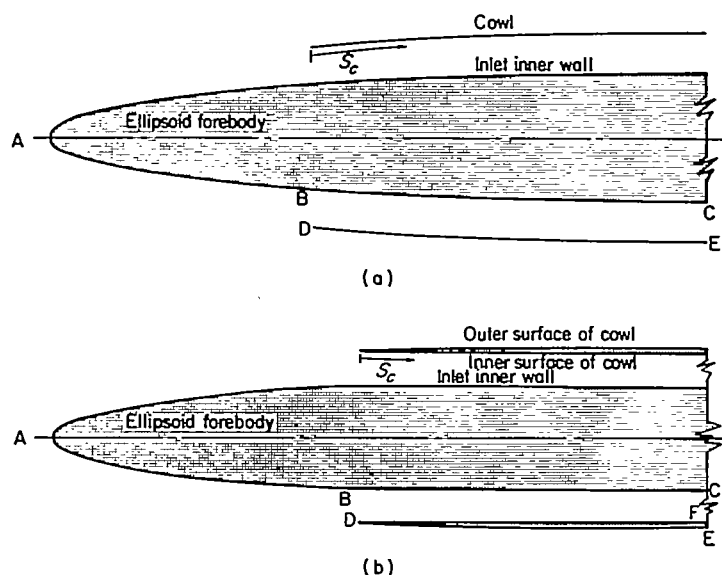
(a) Configuration 1. Inlet velocity ratio, 1.0.
(b) Configuration 2. Inlet velocity ratio, 0.7.
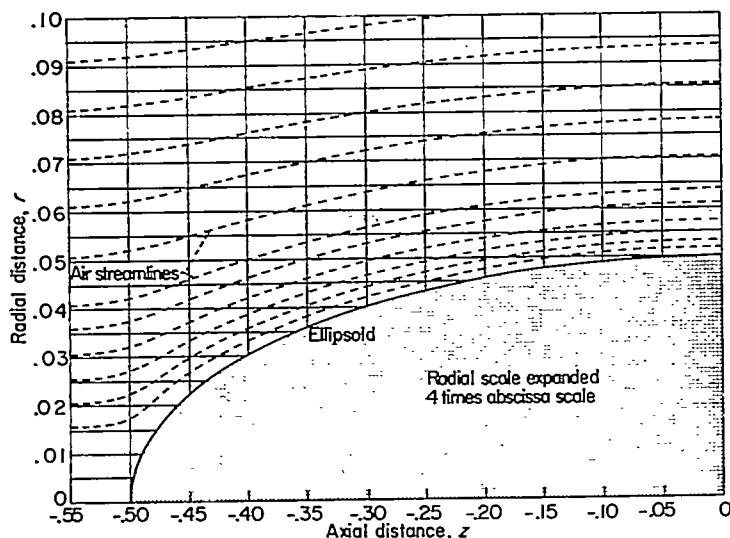
FIGURE 1.—Inlet configurations.

FIGURE 2.—Air streamlines surrounding 10-percent-thick ellipsoid. (A large working copy of this figure may be obtained on request from NACA Headquarters, Washington, D. C.)

Each of the two configurations has an associated inlet velocity ratio, which is defined as the ratio of the velocity at the inlet entrance to the free-stream velocity. For configuration 1 the inlet velocity ratio is nominally 1.0. (Precise calculations show that the inlet velocity ratio may vary from 0.98 to 1.02, depending on the location of the inlet entrance.) The inlet velocity ratio for configuration 2 is nominally 0.7 (0.714, actually). A particular airflow field is associated with each velocity ratio. The methods used in calculating the two flow-field patterns produced a cowl and inner wall with a slight difference in geometrical shape for the two inlets. In spite of this, the difference in velocity ratio is not caused principally by the difference in geometry, but rather by differences in airflow requirements through the inlets. As will be discussed further, the slight cowl thickness of configuration 2 will not appreciably affect the amount of water ingested; thus, the two inlets may be compared on the basis of velocity ratio.

INLET WITH VELOCITY RATIO OF 1.0

The droplet impingement on the cowl and the amount of water ingested can be obtained by extending the analysis of the trajectory calculations made for the results reported in references 2 and 4. Droplet trajectories in space surrounding the 10- and 20-percent-thick ellipsoids were calculated in order to obtain the results reported in references 2 and 4 on spatial variation of local liquid-water concentration. These same trajectories are not altered by an inlet such as shown in figure 1(a) if the air streamlines (or airflow field) ahead of and surrounding the ellipsoid are not altered by the inlet. The placement of an inlet around the

ellipsoid (or around a sector between two meridian planes) will not alter the airflow field if the cowl is of negligible thickness, the cowl contour coincides with that of the air streamline on which it is superposed, and the values of local air velocity around the ellipsoid are not changed. The provision that the local velocity is not changed implies that the airflow remains ideal and without viscosity or boundary layers at the inlet walls.

The example shown in figure 1(a) illustrating the geometrical configuration discussed in the preceding paragraphs has the forebody ABC defined by the equation $z^2+100r^2=0.25$. This is the equation for a 10-percent-thick ellipse located with zero coordinates at the midpoint. The outer wall DE of the inlet is given by the equation for the air streamlines:

$$\psi=\frac{1}{2}\frac{2\alpha}{L}(1-\mu_1^2)(\lambda^2-1)\left[\frac{1}{2}\ln\left(\frac{\lambda+1}{\lambda-1}\right)-\frac{\lambda}{\lambda^2-1}\right]\times$$

$$\frac{-\frac{1}{2}}{\frac{1}{2\epsilon}\ln\left(\frac{1+\epsilon}{1-\epsilon}\right)-\frac{1}{1-\epsilon^2}}+\frac{1}{2}\left(\frac{2\alpha}{L}\right)^2(1-\mu_1^2)(\lambda^2-1) \quad (1)$$

(Symbols are defined in appendix A.)

Air streamlines are shown as dashed lines in figure 2. A much simpler equation of the form

$$z^2+cr^2=g \quad (2)$$

applies very well over the region between $z=-0.4$ and $z=0$. The ordinate scale r in figure 2 is expanded to 4 times the abscissa scale z in an effort to obtain precision. This scale distortion is used in several subsequent figures presenting trajectory data.

Trajectories of droplets are shown in figure 3. Droplets shown starting at infinity at points j and k impinge on the
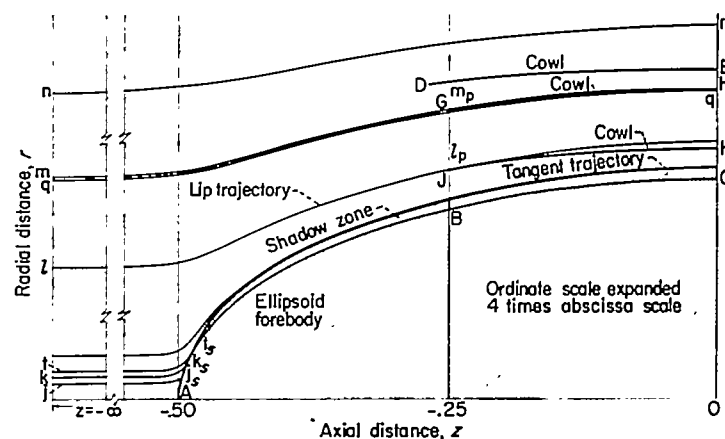

FIGURE 3.—Illustration of droplet trajectories with respect to three possible locations of inlet walls.

forebody at points j_s and k_s, respectively, and are assumed to be removed from the possibility of entering the inlet. The trajectory with starting point t is tangent to the forebody at t_s and continues in space around the elliptical forebody. Between the tangent trajectory and the forebody is a region void of droplets commonly referred to as the shadow zone.

Three possible entrance walls are shown in figure 3. The choice of either entrance wall JK or GH or any other wall such as DE (fig. 3) that coincides with an air streamline (fig. 2) depends on entrance-size requirements. If an entrance wall such as JK (fig. 3) meets the entrance-size requirements, then all the droplets in the space between the tangent trajectory and the entrance lip trajectory l–l_p will be ingested. (This discussion applies only to clouds made of droplets of uniform size. The concept involving clouds with a distribution, or spectrum, of droplet sizes is discussed in ref. 5.) The space between the trajectories is bounded by the surfaces formed by rotating the trajectories in the r,z-plane about the axis of the ellipsoid. With the entrance wall placed at GH, trajectories such as n–n with starting ordinates r_0 larger than those for m–m_p will miss the forebody and entrance altogether. The liquid water in droplet form in the annulus space between trajectories m–m_p and q–q will impinge on the inner surface of wall GH between $z=-0.25$ and 0. The detailed method for finding both the amount of water ingested and the water distribution is shown with examples in a subsequent section.

INLET WITH VELOCITY RATIO OF 0.7

The solution of the airflow field for an inlet velocity ratio other than 1.0 was obtained in a median plane by adding a two-dimensional perturbation field representing the effect of the inlet to the r- and z-components of the air velocity field surrounding a 10-percent-thick prolate ellipsoid of revolution. The addition of a two-dimensional perturbation field to a three-dimensional field confined to one meridian plane is not strictly correct. This method of solution is justified only if the two-dimensional perturbation is not large and if the inlet is located where the radial component of flow is small—that is, not near the nose of the ellipsoid. The two requirements are complied with in the solution for this problem, because the strength of the perturbation reduces the velocity ratio to only 0.7 and the inlet is located outside the ellipsoid in a region of largest ellipsoidal diameters.

The perturbation field used in this study is derived and discussed in appendix B. The boundary conditions at the surfaces of the forebody and inlet walls are satisfied, because these surfaces represent air streamlines after the perturbation velocities are added to the basic flow-field velocities of the 10-percent-thick ellipsoid. The resulting configuration (fig. 1(b)) has an attendant flow field that was used in the calcu-

lation of the trajectories. Unlike the preceding case for a velocity ratio of 1.0, the cowl is fixed in its location with respect to the inner wall and centerline of the forebody, and only one configuration is associated with this inlet velocity ratio of 0.7.

The forebody and inlet inner wall ABC (fig. 4) are defined parametrically by

$$-z=0.00943\ (\varphi+0.995e^{\varphi})+0.2780$$

$$r=0.00943\ (0.1+0.0998e^{\varphi})+0.0418$$

for values of φ between 0.6 and -29.5. This curve approaches $r=0.041$ between $z=-0.25$ and $z=0$, and very closely approximates an ellipse between $z=-0.30$ and $z=-0.47$. In order to simplify the concepts and the presentation of the data, the forebody AB in figure 4 and all subsequent figures illustrating this inlet is the 10-percent-thick ellipse defined by the equation $z^2+100r^2=0.25$. The outer wall DE of the inlet is defined by a section of the ellipse $z^2+133r^2=0.75$. The inner surface DF of the cowl is the line $r=0.0714$.

As in the case for a velocity ratio of 1.0, the amount of water ingested into the inlet is the water contained in the space between the tangent trajectory (t–t_s, fig. 4) and the trajectory that intersects the entrance lip on the cowl of the inlet (l–l_p, fig. 4).

DETERMINATION OF DROPLET PATH

The method for the determination of the droplet path is essentially the same as is described in reference 5. Assumptions that are necessary to the solution of the problem are: (1) At a large distance ahead of the body the droplets are at rest with respect to the air; (2) the only external force acting on the droplets is the drag force due to the relative velocity of the air with respect to the droplets; and (3) the droplets are always spherical and do not change in size.
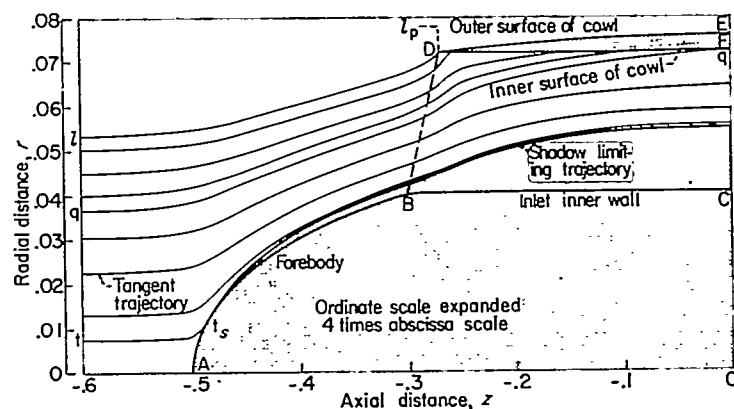

FIGURE 4.—Illustration of droplet trajectories with respect to 0.7-velocity-ratio inlet.

DIFFERENTIAL EQUATIONS OF DROPLET MOTION

The differential equations that describe the motion of the droplets were obtained by equating the drag force with the rate of change of momentum of the droplet (ref. 5). The equations are expressed in dimensionless form in order to maintain the number of calculations at a minimum and to simplify the presentation of the results. Since a flow field is axisymmetric around an ellipsoid of revolution oriented at 0° between its major axis and the direction of the free stream, the droplet trajectories in all meridian planes are the same. The dimensionless equations of motion of the droplet trajectories are of the same form as those derived in reference 5 and can be written

$$\left.\begin{array}{l} \dfrac{dv_r}{d\tau}=\dfrac{C_D Re}{24}\dfrac{1}{K}(u_r-v_r) \\[2mm] \dfrac{dv_z}{d\tau}=\dfrac{C_D Re}{24}\dfrac{1}{K}(u_z-v_z) \end{array}\right\} \qquad (3)$$

where Re is the local Reynolds number with respect to the droplet diameter $2a$ and the local relative velocity between the air and the droplet. Thus,

$$Re=\frac{2a\rho_a U^*}{\mu}\sqrt{(u_r-v_r)^2+(u_z-v_z)^2} \qquad (4)$$

The coefficient in equation (4) is called the free-stream Reynolds number Re_0; hence,

$$Re_0=\frac{2a\rho_a U^*}{\mu} \qquad (5)$$

The dimensionless number K, the inertia parameter, is defined as follows:

$$K=\frac{2}{9}\frac{\rho_w a^2 U^*}{\mu L} \qquad (6)$$

The coefficient of drag C_D may be obtained from experimental data as a function of the local droplet Reynolds number Re.

An examination of equations (3) and (4) shows that the characteristics of the trajectories depend only on the values of the two dimensionless parameters K and Re_0. Thus, a unique set of droplet trajectories exists for every combination of K and Re_0.

METHOD OF SOLUTION

The differential equations of motion (3) are difficult to solve, because values of the velocity components and the factor containing the coefficient of drag depend on the position and velocity of the droplet at each instant and therefore are not known until the trajectory is traced. The values of these quantities must be fed into the equations as a trajectory is developed. This was accomplished by using a mechanical differential analyzer constructed at the NACA Lewis laboratory for this purpose (ref. 6). The results were obtained in the form of plots of droplet trajectories in the coordinates of figures 3 and 4.

The following information was required for use with the differential analyzer in the trajectory calculation:

(1) Coefficient-of-drag data: Values of the factor $C_D Re/24$ as a function of Re were obtained from tables in reference 7.

(2) Air velocity components: The air velocity components u_r and u_z were determined as functions of r and z by means of an analytical solution of the three-dimensional flow field ahead of an ellipsoid for the case of the inlet with a velocity ratio of 1.0 (ref. 1) and by the method described in appendix B for the inlet with a velocity ratio of 0.7.

(3) Starting conditions: Before the integration could be performed with the differential analyzer, the initial velocity of the droplets had to be determined at the point selected as the starting position. In addition, since the starting position must be selected at a finite distance ahead of the ellipsoid, it was necessary to make a correction to this starting ordinate in order to obtain the corresponding starting ordinate r_0 at $z=-\infty$. The procedure for obtaining the starting conditions for the analog is the same as that discussed in detail in reference 1.

The equations of motion (eq. (3)) were solved for various values of the parameter $1/K$ between 0.1 and 90. The inertia parameter K is a measure of the droplet size, the flight speed, the size of the basic ellipsoid, and the viscosity of the air. In convenient dimensions, it is written in the form

$$K=1.704\times10^{-12}\frac{d^2 U}{\mu L} \qquad (7)$$

The density of water, which is expressed as part of the conversion factor, is 1.94 slugs per cubic foot.

For each value of the parameter $1/K$, a series of trajectories was computed for each of several values of free-stream Reynolds number Re_0. In convenient dimensions, the free-stream Reynolds number with respect to the droplet diameter is written as

$$Re_0=4.813\times10^{-6}\frac{d\rho_a U}{\mu} \qquad (8)$$

In order to make these dimensionless parameters more physically significant in the following discussion, some typical combinations of K and Re_0 are presented in table I for various lengths and velocities of the basic ellipsoid, droplet sizes, and flight pressure altitudes and temperatures. A procedure for rapid calculation of $1/K$ and Re_0 from practical flight conditions is given in appendix B of reference 8.

RESULTS AND DISCUSSION
INLET WITH VELOCITY RATIO OF 1.0

Several sets of trajectories for different combinations of Re_0 and $1/K$ are shown in figure 5 for a 10-percent-thick ellipsoid. Some of the many possible wall locations are shown in figure 5 as dashed lines, which are duplications of the air streamlines shown in figure 2. The cowl lip may be located anywhere along the air streamline. The trajectories are shown as medium-weight solid lines. The order of presentation of figures 5(a) to (e) is in accordance with the amount that droplet trajectories differ from air streamlines. That is, in figure 5(a) the difference between a droplet trajectory and a superposed air streamline (particularly regarding the slope of each at a given point in space) is greater than in figure 5(e). In figure 5(e) the directions of the droplet trajectories are everywhere nearly coincident with air streamlines. This order of presentation also shows the correlation between droplet impingement on the cowl and the parameters Re_0 and $1/K$. The impingement in figure 5(d) is less than in figures 5(a) or (b).
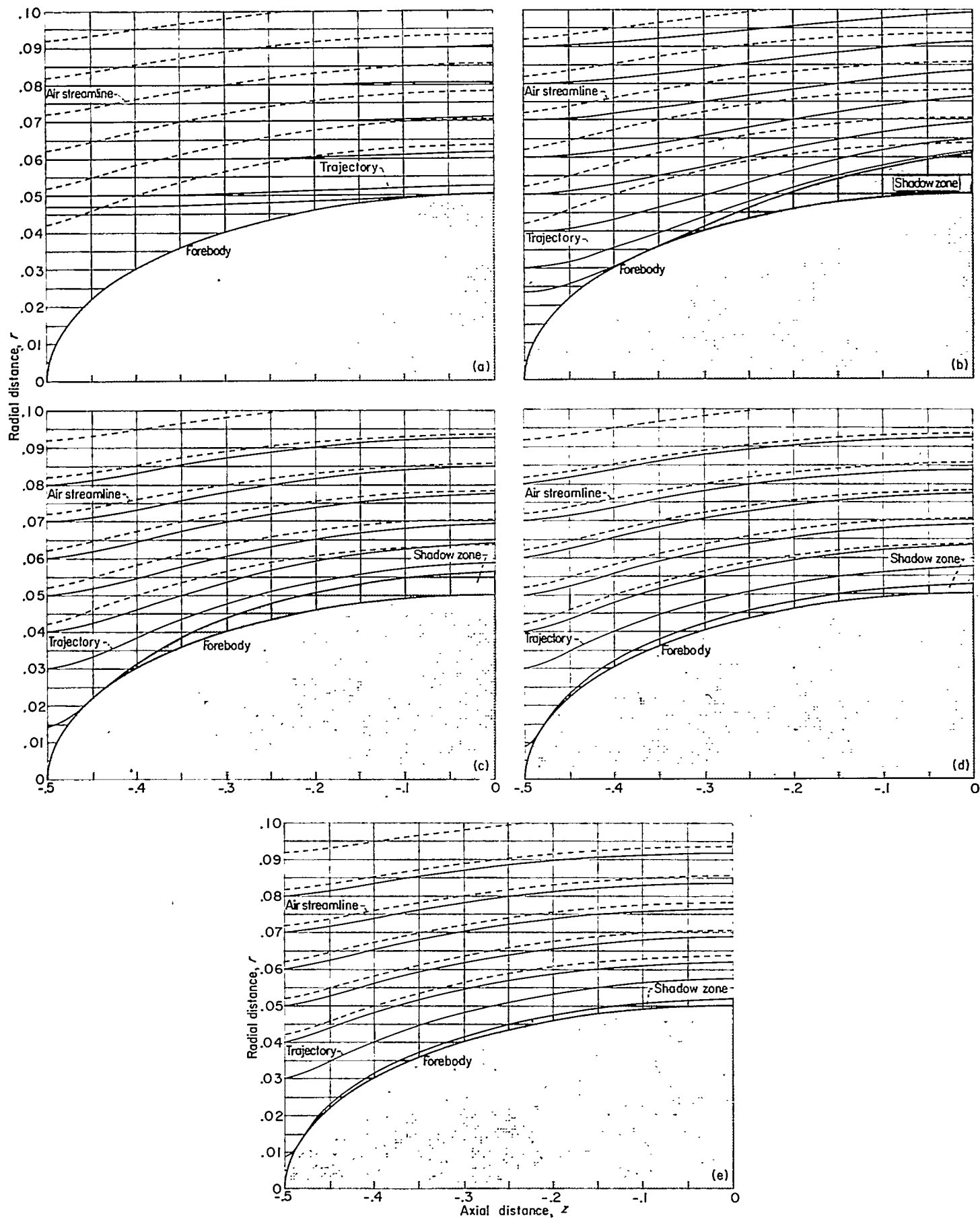
(a) $1/K=1/30$; $Re_0=8192$.   (b) $1/K=3$; $Re_0=512$.
(c) $1/K=15$; $Re_0=128$.   (d) $1/K=45$; $Re_0=128$.

(e) $1/K=114$; $Re_0=8$.

FIGURE 5.—Trajectories for inlet with velocity ratio of 1.0.   Basic ellipsoid, 10 percent thick.

The significance in the variation of $1/K$ and Re_0 is seen in table I. Some of the approximate possible flight and atmospheric combinations that could be applied to figure 5 are given in the following table:

Flight speed, mph	Pressure altitude, ft	Droplet diam., d, microns	Ellipsoid major axis, L, ft	Reciprocal of inertia parameter, $1/K$	Free-stream Reynolds number, Re_0	Figure 5
300	5,000	1000	50	1/30	8192	(a)
	15,000	80	29	3	512	(b)
		20	10	15	128	(c)
			27	45	128	(d)
50	25,000	10	3	114	8	(e)

Droplet ingestion.—The amount of water ingested by an inlet is the water in droplet form through an annular area of

space (perpendicular to the major axis of the ellipsoid) between the inlet lip and the body of the ellipsoid. For example, if the inlet cowl were located at JK in figure 3, water would be ingested through an annular area of space of width BJ. For the case of a velocity ratio of 1.0, wherein any number of locations of the cowl are possible, the amount of water ingested must be presented as a function of inlet entrance location as well as Re_0 and $1/K$.

If, for a particular combination of values of Re_0 and $1/K$, the point of tangency t_s of the tangent trajectory occurs outside the entrance, such as in figure 3 (i. e., the z-position of the point of tangency is upstream of the z-position of the entrance lip), the amount of water ingested is obtained from the following equation:

$$W_i = 0.33\pi w_0 L^2 U(r_{0,t}^2 - r_{0,tan}^2) \tag{9a}$$
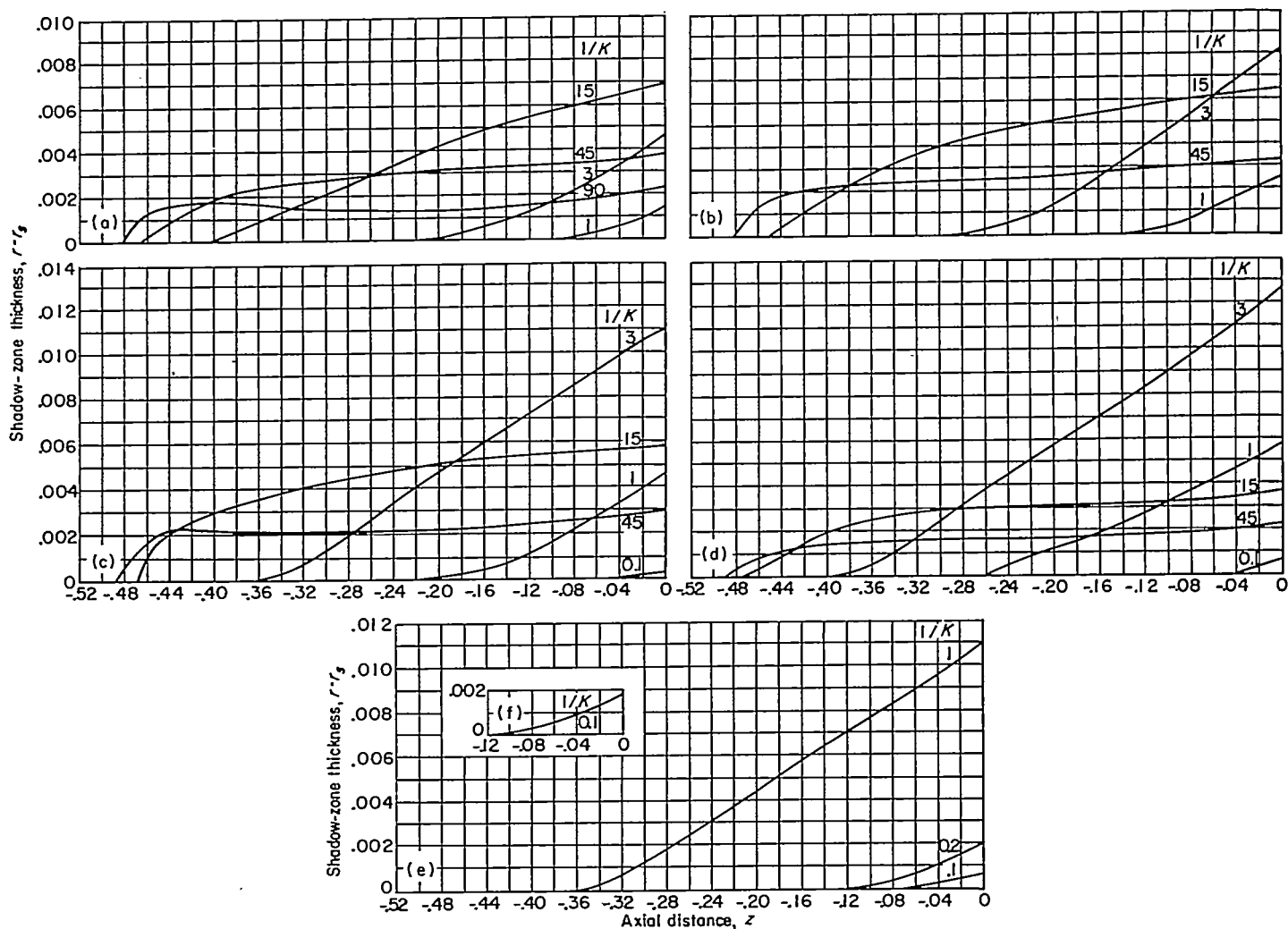
(a) Free-stream Reynolds number, 0.
(b) Free-stream Reynolds number, 128.
(c) Free-stream Reynolds number, 512.
(d) Free-stream Reynolds number, 1024.
(e) Free-stream Reynolds number, 4096.
(f) Free-stream Reynolds number, 8192.

FIGURE 6.—Thickness of shadow zone as function of axial position. Basic ellipsoid, 10 percent thick; inlet velocity ratio, 1.0.

(a) $z=0$; $Re_0=0$.
(c) $z=0$; $Re_0=512$.
(e) $z=0$; $Re_0=4096$.

(b) $z=0$; $Re_0=128$.
(d) $z=0$; $Re_0=1024$.
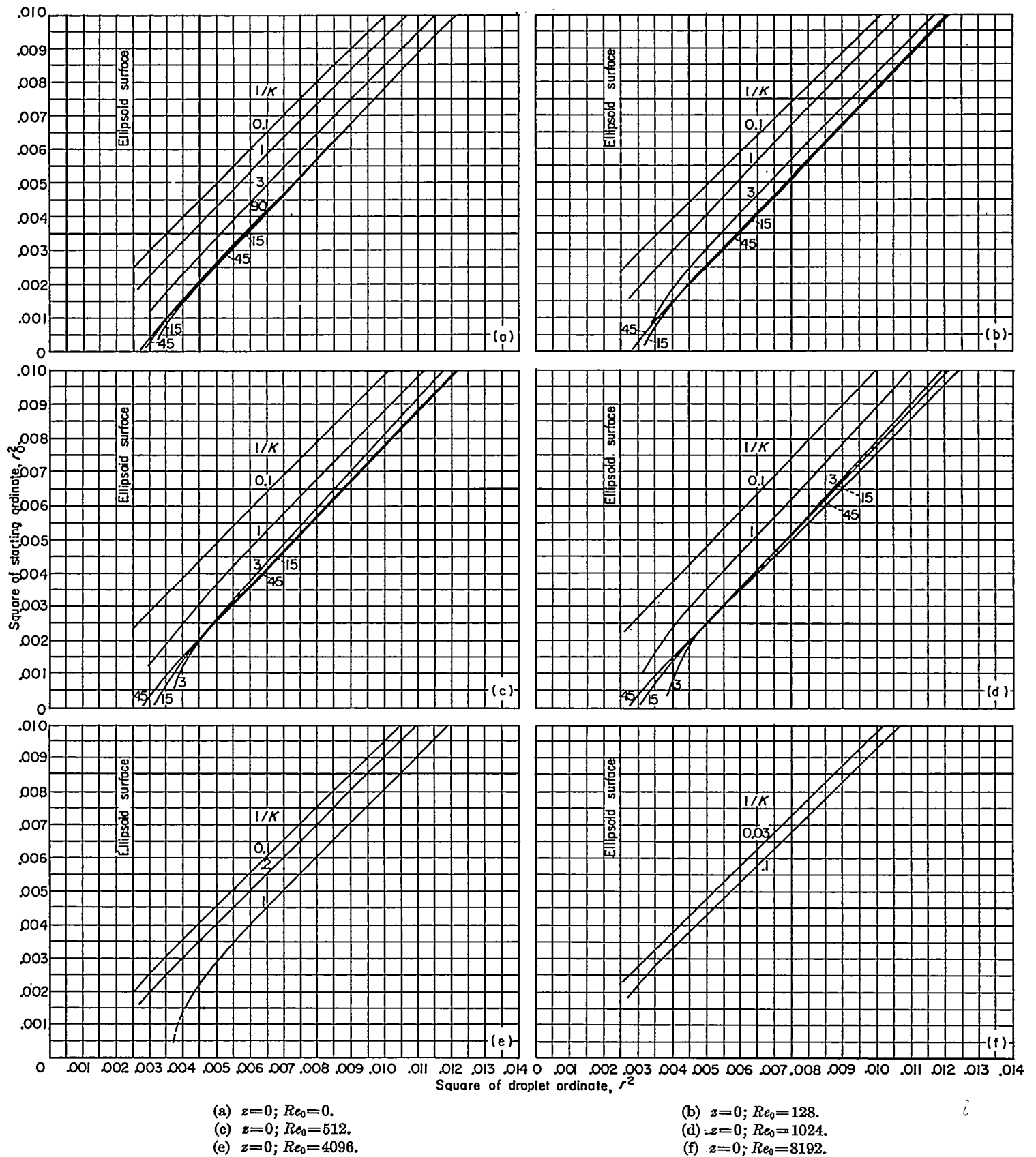(f) $z=0$; $Re_0=8192$.

FIGURE 7.—Square of starting ordinate as function of square of droplet ordinate at constant axial position. Basic ellipsoid, 10 percent thick; inlet velocity ratio, 1.0.

(g) $z=-0.25$; $Re_0=0$.
(i). $z=-0.25$; $Re_0=512$.
(k). $z=-0.25$; $Re_0=4096$.

(h) $z=-0.25$; $Re_0=128$.
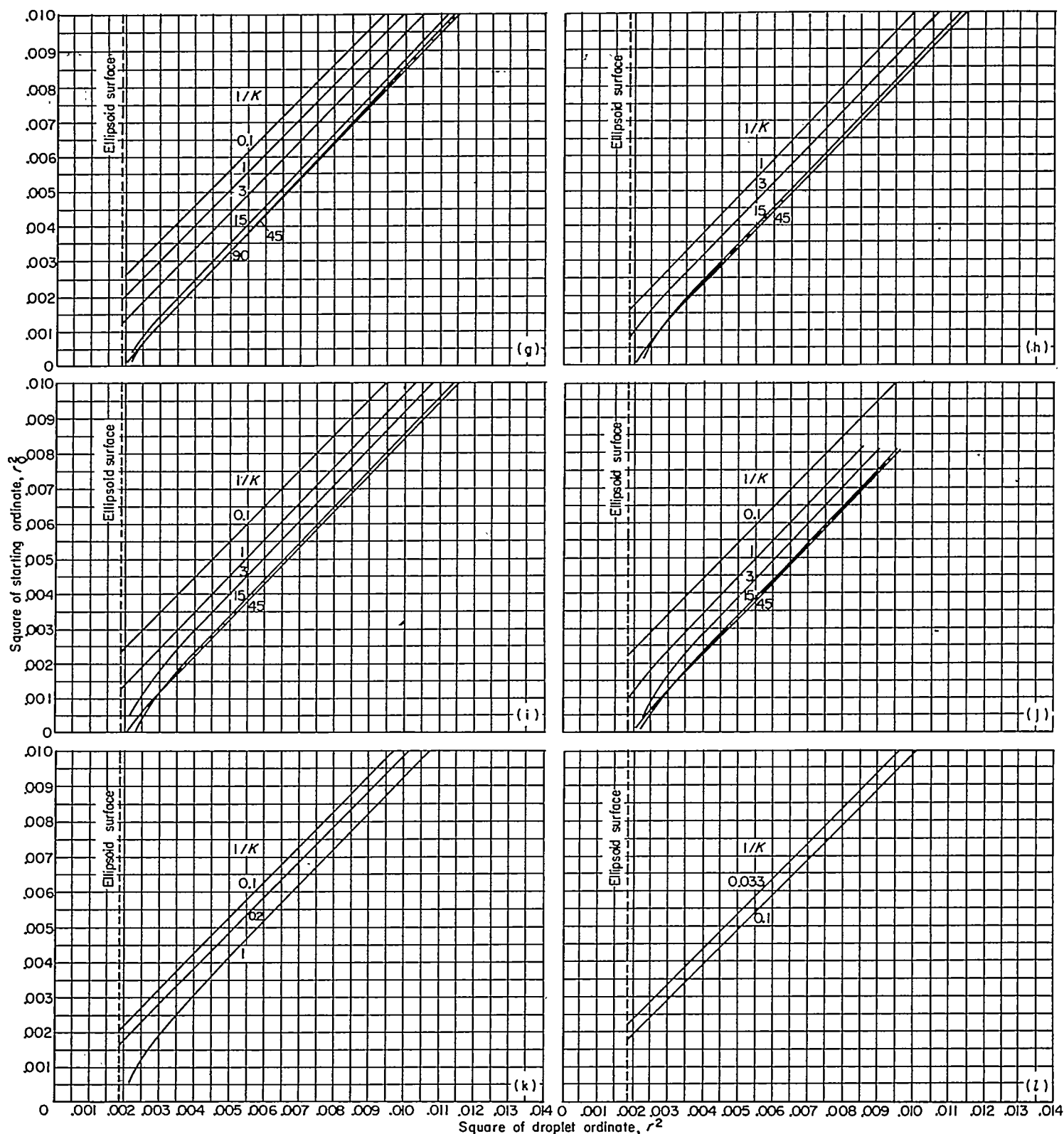(j) $z=-0.25$; $Re_0=1024$.
(l) $z=-0.25$; $Re_0=8192$.

FIGURE 7.—Continued. Square of starting ordinate as function of square of droplet ordinate at constant axial position. Basic ellipsoid, 10 percent thick; inlet velocity ratio, 1.0.

where $r_{0,l}$ is the free-stream radial distance at $z=-\infty$ of the trajectory that touches the entrance lip, and $r_{0,tan}$ is the free-stream radial distance of the tangent trajectory. If the tangency point is located downstream of the entrance lip (i. e., inside the entrance, see fig. 5 (a)), the water ingested is obtained from

$$W_i=0.33\pi w_0 L^2 U(r_{0,l}^2-r_{0,B}^2) \qquad (9b)$$

where $r_{0,B}$ is the radial distance at $z=-\infty$ of the trajectory that impinges on the ellipsoid at the same z-position as the inlet opening, such as point B in figure 3. The z-position of the tangent trajectory can be obtained from figure 6, which is a reproduction of figure 8 of reference 4. The z-position of the tangency corresponds in figure 6 to the zero value of the shadow-zone thickness $r-r_s$. The amount of water ingested for various radial locations of the lip can be found from the data presented in figure 7, which is a reproduction of figure 4 of reference 4, if the inlet lip is located at $z=0$, -0.25, or -0.50. Intermediate locations of the entrance lip may be treated by cross-plotting the data in figure 7.

The following example illustrates the use of figure 7. Assume flight and atmospheric conditions such that $Re_0=128$ and $1/K=45$. These conditions correspond to an approximate flight speed of 300 miles per hour, cloud-droplet diameter of 20 microns, ellipsoid length of 27 feet, and pressure altitude of 15,000 feet. Further, assume that design criteria governing the inlet spacing area place the inlet lip at $r=0.08$ and $z=-0.25$. Figure 7(h) is used to obtain the required values of $r_{0,l}^2$ and $r_{0,tan}^2$.

From figure 7(h), the value of $r_{0,l}^2=0.00477$ is found from the curve for $1/K=45$ for an abscissa reading of $r^2=(0.08)^2=0.0064$. The value of $r_{0,tan}^2$ can be obtained from the same figure by reading the bottom end of the same curve. For this example, $r_{0,tan}^2=0.000045$. The only remaining unknown for the solution of equation (9a) is the liquid-water content w_0, which can be obtained from meteorological data. The bottom ends of the curves of figure 7 automatically give either the value of $r_{0,tan}^2$ or $r_{0,B}^2$, whichever applies. If the bottom ends of the curves touch the dashed line labeled "ellipsoid surface," $r_{0,B}^2$ is obtained; whereas $r_{0,tan}^2$ is obtained from the curve ends that do not touch the dashed line.

If the cowl lip is located at $z=-0.50$ and the cowl coincides with an air streamline, the water ingested can be obtained from the data in figure 7(m). The procedure for determining the water ingested is the same as in the preceding example, except that

$$W_i=0.33\pi w L^2 U r_{0,l}^2 \qquad (9c)$$

because the lower limiting trajectory coincides with the z-axis.

The method described for obtaining the amount of water ingested pertains in principle to a simple configuration in which a portion of an air streamline is replaced by a wall of negligible thickness. In an actual model, the wall has thick-

ness and probably deviates from an air streamline. The method still applies if the wall thickness is not large compared with the ellipsoid thickness, which is usually the case, and the centerline of the wall shape approximates an air streamline. In other words, the results obtained by this method are not sensitive to small deviations from the ideal model presumed in these studies, because small amounts of wall thickness and wall deviation from the original shape of the air streamline introduce only small changes in the air streamline pattern. Furthermore, because of the droplet inertia, the change in droplet trajectory is even less than the change in air streamline pattern.

Total impingement on inlet walls.—The amount of water impinging on the inlet walls is a function of the inlet lip position as well as of the values of $1/K$ and Re_0. If the point of tangency t_s is outside (upstream of) the entrance opening (fig. 3), there is no impingement on the inner wall of the inlet. The z-position of the point of tangency t_s, which corresponds to zero value of shadow zone, is given in figure 6.

If the point of tangency occurs inside the entrance, the amount of water impinging on the inlet inner wall (i.e., on the ellipsoid surface downstream of the inlet opening) can be found from the studies reported in reference 3. The water impinging on the ellipsoid surface between the entrance opening and the point of tangency t_s on the inlet inner wall is

$$W_{B-t_s}=1.04 w_0 L^2 U(r_{0,tan}^2-r_{0,B}^2) \qquad (10)$$

where 1.04 is the combination of constants in equation (9). The value of $r_{0,tan}^2$ is available directly in figure 8. The value for $r_{0,B}^2$ can be obtained from figure 9. A correlation between z and the distance S along the ellipsoid surface for use in connection with figure 9 is available in figure 10.

Whether impingement occurs on the outside surface of the cowl depends primarily on the values of $1/K$ and Re_0.
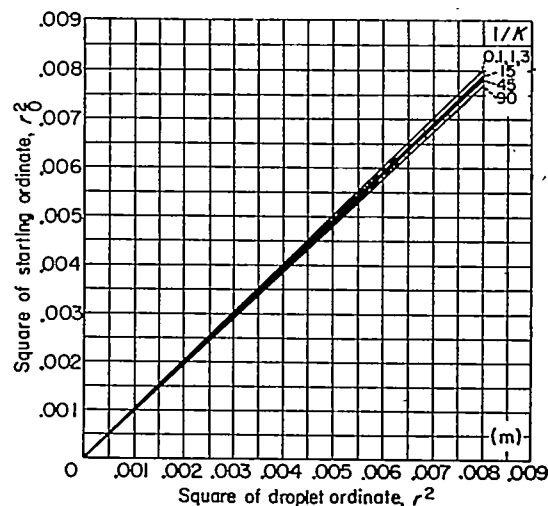
(m) $z=-0.50$; $Re_0=0$, 128, 512, 1024, 4096, and 8192.
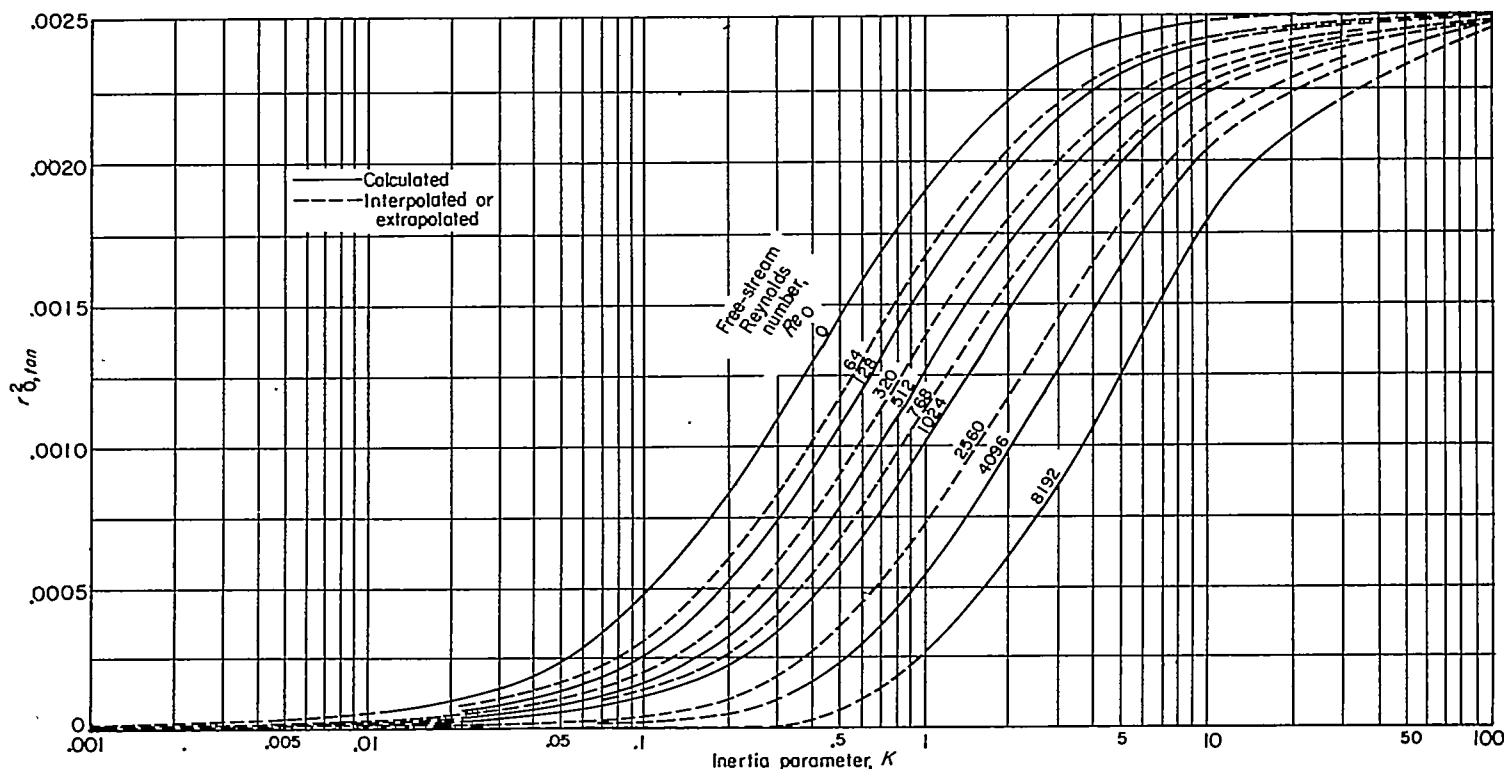
FIGURE 7.—Concluded.

FIGURE 8.—Square of starting ordinate of tangent trajectory as function of inertia parameter. Basic ellipsoid, 10 percent thick; inlet velocity ratio, 1.0.

For example, the trajectories shown in figure 5(a) are nearly straight lines. For the conditions represented by figure 5(a), impingement occurs only on the outside surface of the cowl. For conditions represented in figure 5(b), the amount of impingement on the outside and inside cowl surfaces depends on the r- and z-position of the inlet lip. For conditions represented in figures 5(c) to (e), impingement occurs only on the inside surface.
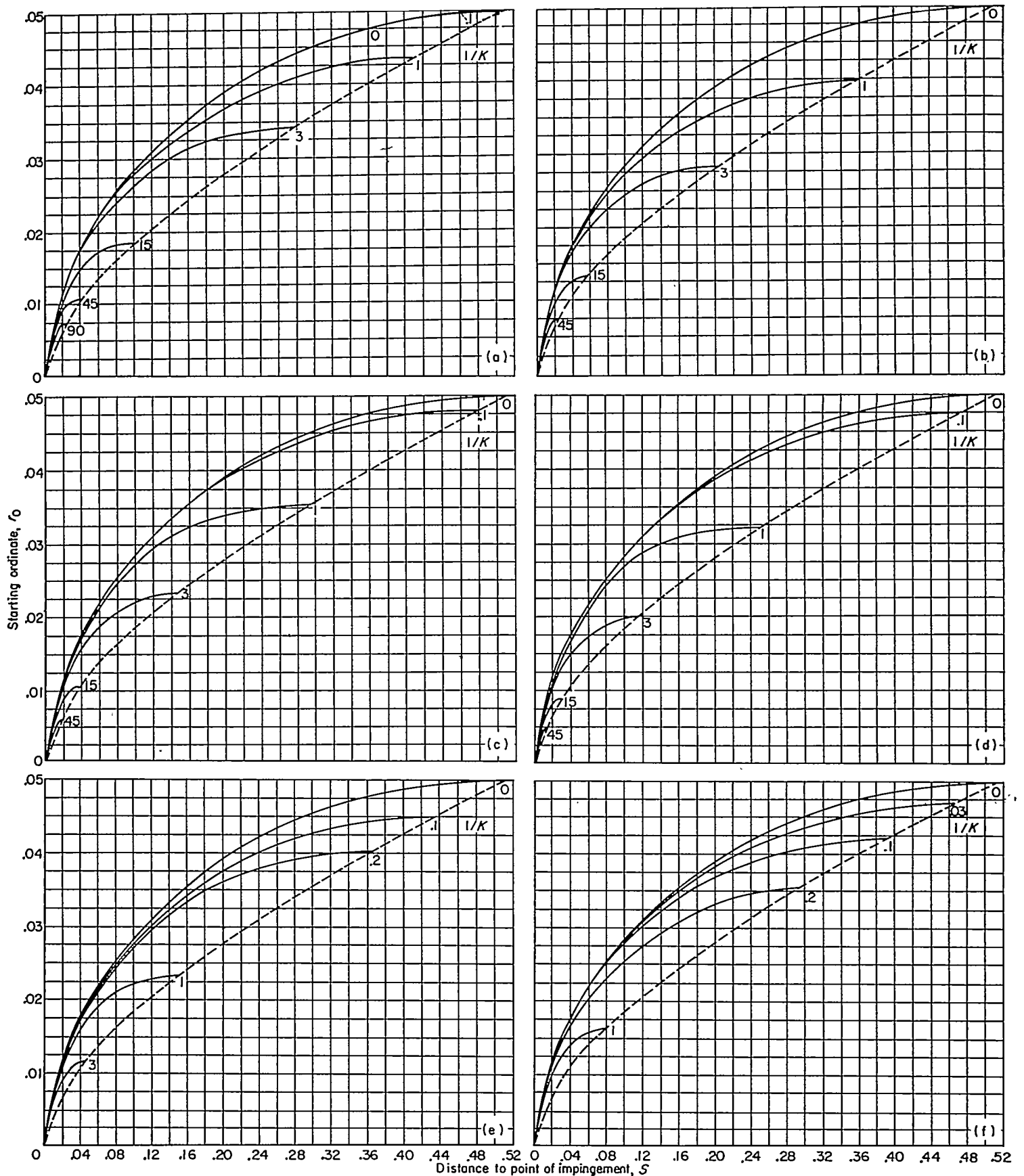
Figures 5(a) and (e) represent the two extremes of trajectory shape. Combinations of values of $1/K$ less than 1/30 with Re_0 less than 8192 result in trajectories at least as straight as those shown in figure 5(a). Combinations of values of $1/K$ greater than 114 with Re_0 greater than 8 result in trajectories that follow the air streamlines at least as well as those shown in figure 5(e). For values of $1/K$ less than 3, the impingement is principally on the outside surface of the cowl between $z=-0.50$ and -0.25. For values of $1/K$ greater than 3, the impingement is principally on the inside surface spread thinly over the entire surface.

Impingement distribution on inlet walls.—No attempt is made to give quantitative values of the amount of water impinging on the cowl nor of the distribution of impingement. Both the amount of impingement and the distribution are very sensitive to small changes in the shape of the cowl, particularly for conditions in which the droplet trajectories are nearly like air streamlines (figs. 5(c) to (e)). The use of figure 5 as a guide will lead to useful approximate results when the cowl has some thickness and the cowl mean line can nearly be superposed on an air streamline. For flight and meteorological conditions represented by figures 5(c) to (e), cowl thickness will bring about impingement on the

entrance lip. The collection on the lip will be very high. For these same flight and meteorological conditions, impingement on the outside surface is hardly perceptible. On the inside surface the rate of impingement is slight, but impingement spreads thinly for a considerable distance downstream of the lip.

Impingement for conditions shown in figure 5(a) can be obtained very easily from the geometry, because the trajectories are nearly straight lines. The most difficult problem is presented by conditions shown in figure 5(b). It is helpful to know that, for the conditions shown in figure 5(b), a cowl with thickness does not disturb the trajectories, because the inertial forces of the droplets are relatively large compared with the forces in the airstream available to change their paths. Therefore, inlet walls with small amounts of thickness can be superposed directly on figure 5(b), and the impingement and distribution can be obtained from the resulting geometry.

Variation of liquid water across inlet opening.—The installation of small protruding objects that do not alter the airflow appreciably is often required near the inlet opening. Occasionally, coarse screens are also used. A knowledge of the rate of ice formation on these objects is very valuable. As with the ellipsoids reported in references 2 and 4, a radial variation in the local liquid-water concentration exists in the immediate vicinity of the elliptical forebody. Thus, the local concentration of water varies radially at the inlet opening. The procedure for determining the spatial variation of liquid water is described in detail in references 2 and 4 and is reviewed here for convenience.

(a)　Free-stream Reynolds number, 0.
(c)　Free-stream Reynolds number, 512.
(e)　Free-stream Reynolds number, 4096.

(b)　Free-stream Reynolds number, 128.
(d)　Free-stream Reynolds number, 1024.
(f)　Free-stream Reynolds number, 8192.

FIGURE 9.—Starting ordinate as function of distance along surface to point of impingement.　Basic ellipsoid, 10 percent thick; inlet velocity ratio, 1.0.

Figure 10.—Relation between distance along ellipsoid surface and axial coordinate. Basic ellipsoid, 10 percent thick; inlet velocity ratio, 1.0.
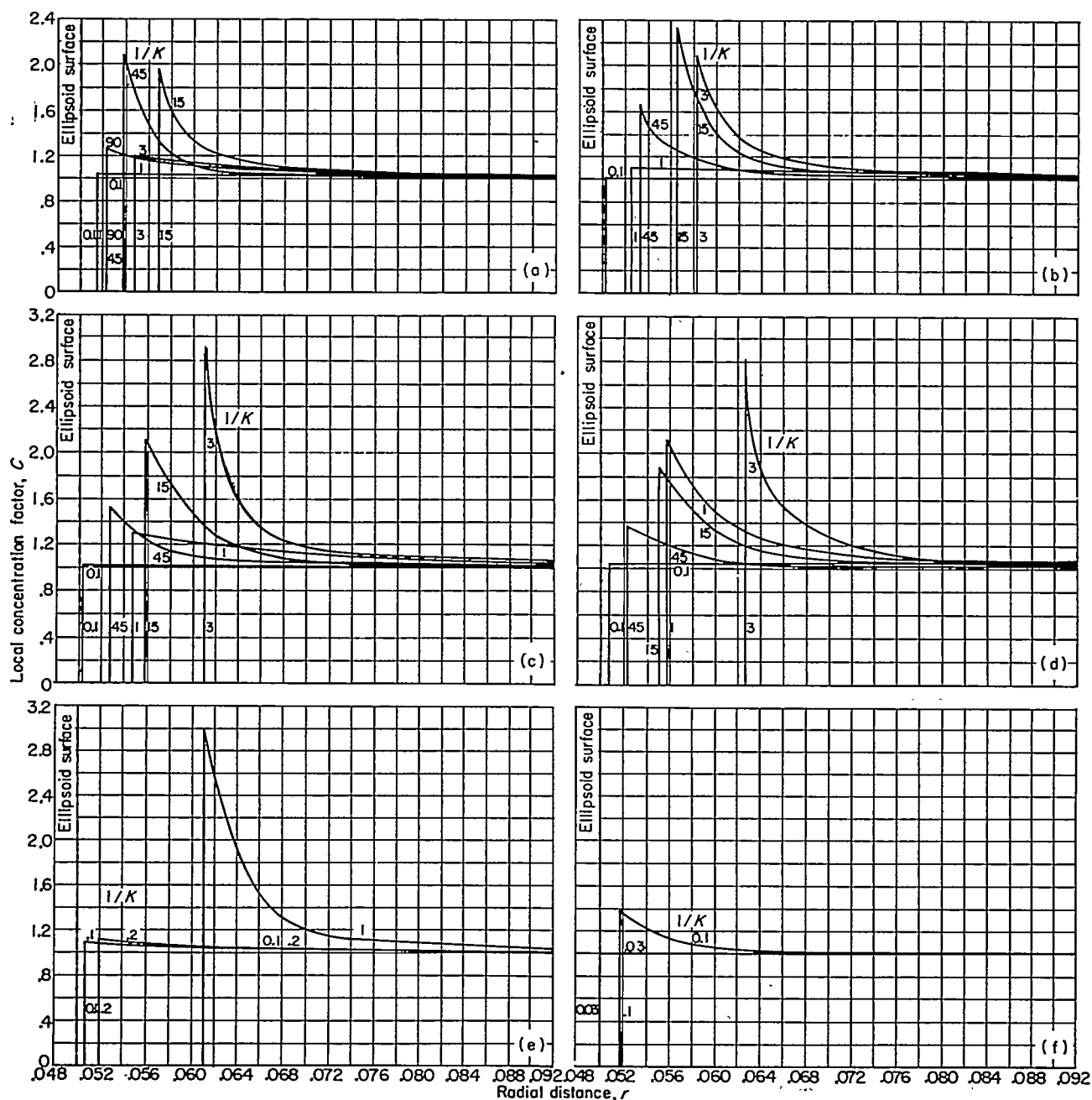
(a) $z=0$; $Re_0=0$.
. (c) $z=0$; $Re_0=512$.
(e) $z=0$; $Re_0=4096$.

(b) $z=0$; $Re_0=128$.
(d) $z=0$; $Re_0=1024$.
(f) $z=0$; $Re_0=8192$.

FIGURE 11.—Variation of local concentration factor with radial distance at constant axial position. Basic ellipsoid, 10 percent thick; inlet velocity ratio, 1.0.

(g) $z=-0.25$; $Re_0=0$.
(i) $z=-0.25$; $Re_0=512$.
(k) $z=-0.25$; $Re_0=4096$.

(h) $z=-0.25$; $Re_0=128$.
(j) $z=-0.25$; $Re_0=1024$.
(l) $z=-0.25$; $Re_0=8192$.
(m) $z=-0.50$; $Re_0=0$, 128, 512, 1024, 4096, and 8192.

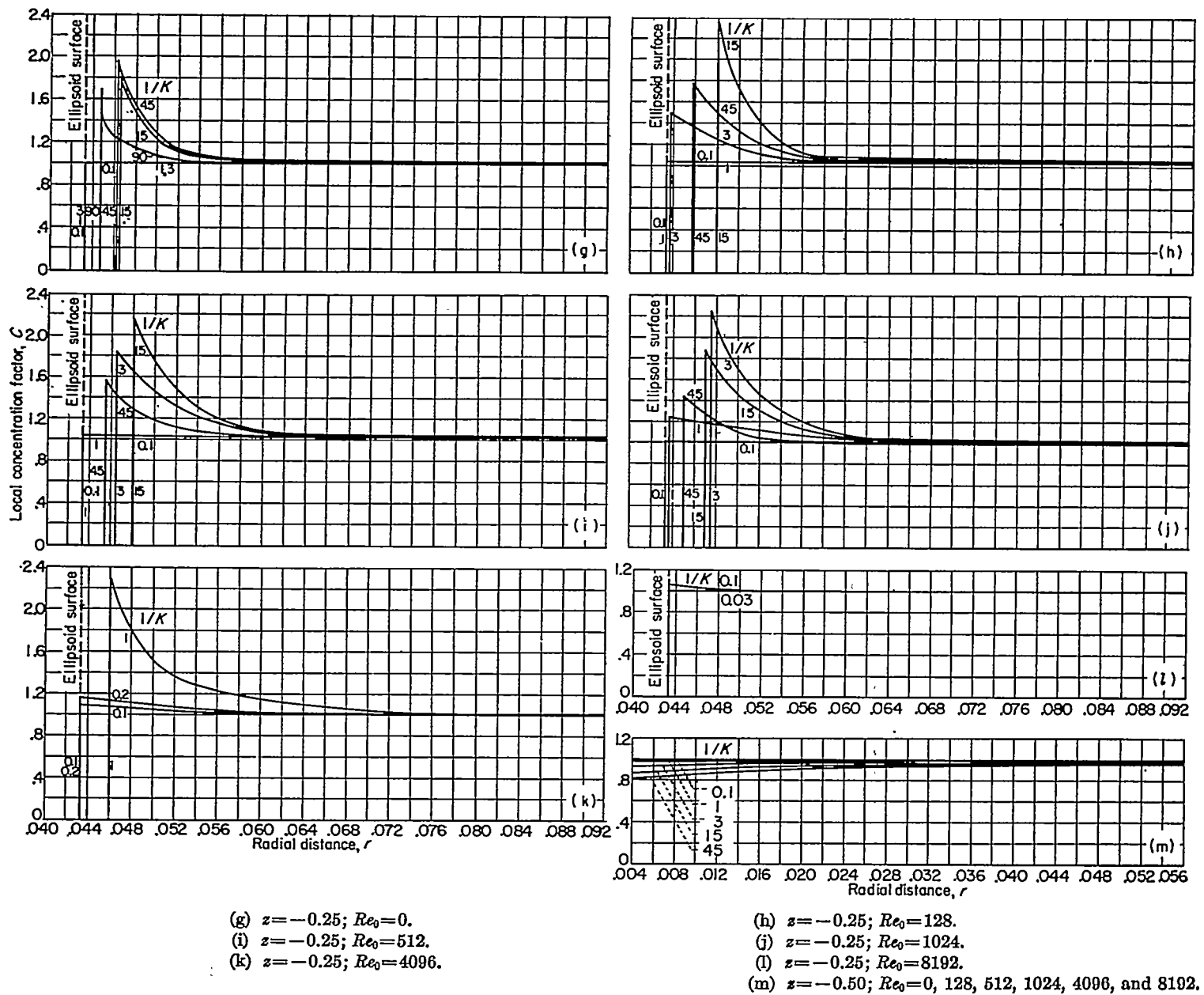FIGURE 11.—Concluded. Variation of local concentration factor with radial distance at constant axial position. Basic ellipsoid, 10 percent thick; inlet velocity ratio, 1.0.

The local weight flux of water in droplet form is

$$F=0.33w_0UC, \text{ lb/(hr)(sq ft)} \qquad (11)$$

where

$$C=\frac{dr_0^2}{dr^2}$$

The element of area implied by the equation is a unit perpendicular to the major axis located in the plane of the inlet opening. The local concentration factor C at a point r in space for three locations of z (0, —0.25, and —0.50) is given in figure 11. The thickness $(r-r_s)$ of the shadow zone

(region of zero concentration) at each z-position on the body is given for various values of Re_0 and $1/K$ in figure 6.

20-Percent-thick ellipsoid.—The preceding results and discussion have been presented for a 10-percent-thick ellipsoid. The same discussion and methods apply to a 20-percent-thick ellipsoid. The corresponding data are available in figures 12 to 18. The air streamlines surrounding a 20-percent-thick ellipsoid are plotted in figure 12. The air streamlines can also be calculated from equation (1). Figure 5 may be used as a guide for estimating the impingement and distribution on the outer wall of the 20-percent-thick body as well as on the 10-percent-thick ellipsoid. The dual use of figure 5 is possible because, relative to the air streamlines, the droplet trajectories are very similar for the two bodies.
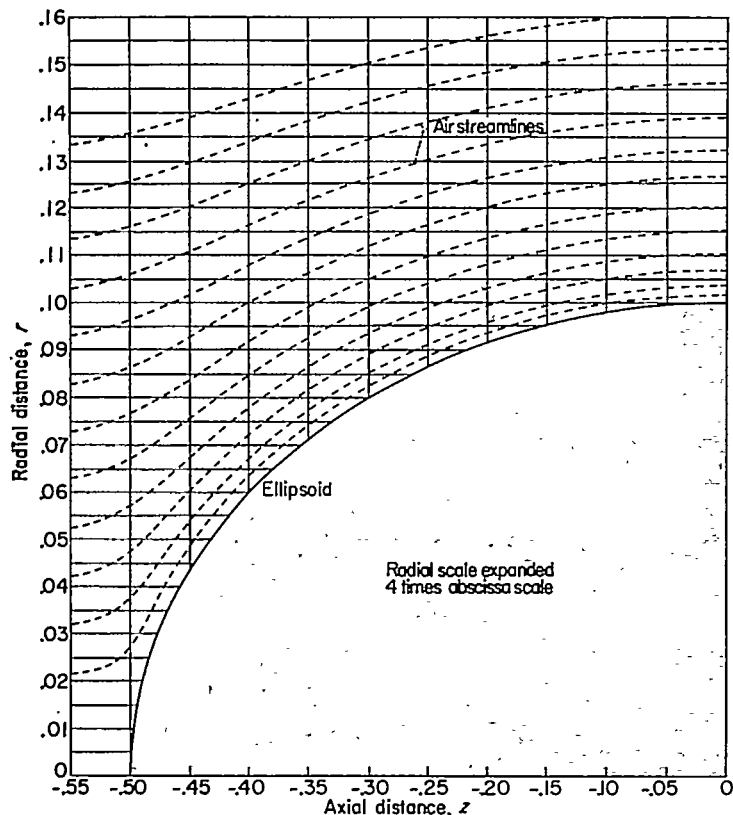
FIGURE 12.—Air streamlines surrounding 20-percent-thick ellipsoid. (A large working copy of this figure may be obtained on request from NACA Headquarters, Washington, D. C.)

FIGURE 15.—Square of starting ordinate of tangent trajectory as function of inertia parameter. Basic ellipsoid, 20 percent thick; inlet velocity ratio, 1.0.

(a) Free-stream Reynolds number, 0.
(c) Free-stream Reynolds number, 512.
(b) Free-stream Reynolds number, 128.
(d) Free-stream Reynolds number, 1024.
(e) Free-stream Reynolds number, 4096.
(f) Free-stream Reynolds number, 8192.

FIGURE 13.—Thickness of shadow zone as function of axial position.   Basic ellipsoid, 20 percent thick; inlet velocity ratio, 1.0.

(a) $z=0$; $Re_0=0$.   (b) $z=0$; $Re_0=128$.
(c) $z=0$; $Re_0=512$.   (d) $z=0$; $Re_0=1024$.
(e) $z=0$; $Re_0=4096$.   (f) $z=0$; $Re_0=8192$.

FIGURE 14.—Square of starting ordinate as function of square of droplet ordinate at constant axial position.   Basic ellipsoid, 20 percent thick; inlet velocity ratio, 1.0.

(g) $z=-0.25$; $Re_0=0$.
(i) $z=-0.25$; $Re_0=512$.
(k) $z=-0.25$; $Re_0=4096$.

(h) $z=-0.25$; $Re_0=128$.
(j) $z=-0.25$; $Re_0=1024$.
(l) $z=-0.25$; $Re_0=8192$.

FIGURE 14.—Continued. Square of starting ordinate as function of square of droplet ordinate at constant axial position. Basic ellipsoid, 20 percent thick; inlet velocity ratio, 1.0.

(m) $z = -0.50$; $Re_0 = 0$.
(o) $z = -0.50$; $Re_0 = 512$.
(q) $z = -0.50$; $Re_0 = 4096$.

(n) $z = -0.50$; $Re_0 = 128$.
(p) $z = -0.50$; $Re_0 = 1024$.
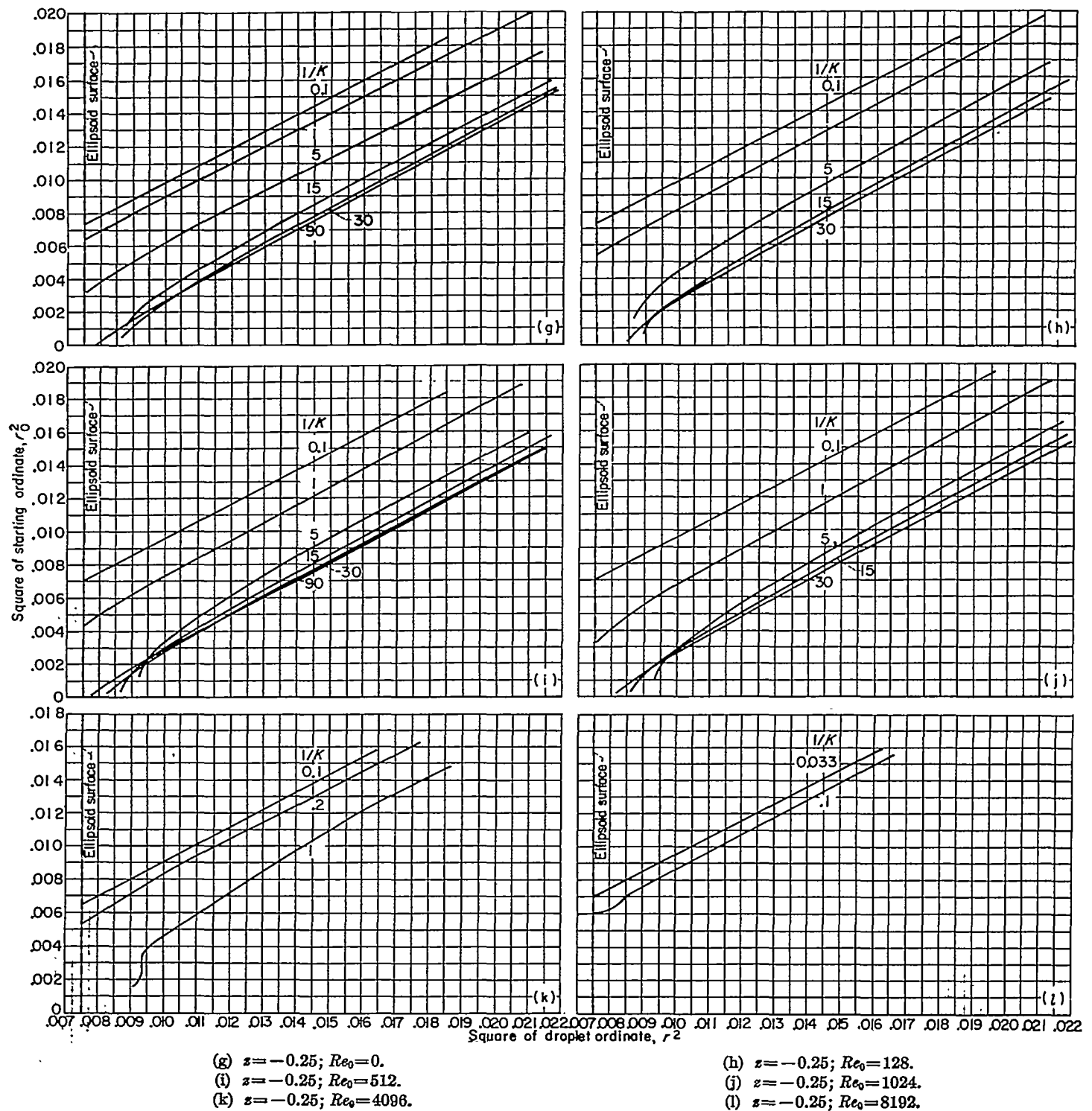(r) $z = -0.50$; $Re_0 = 8192$.

FIGURE 14.—Concluded. Square of starting ordinate as function of square of droplet ordinate at constant axial position. Basic ellipsoid, 20 percent thick; inlet velocity ratio, 1.0.

(a) Free-stream Reynolds number, 0.
(c) Free-stream Reynolds number, 512.
(e) Free-stream Reynolds number, 4096.

(b) Free-stream Reynolds number, 128.
(d) Free-stream Reynolds number, 1024.
(f) Free-stream Reynolds number, 8192.

FIGURE 16.—Starting ordinate as function of distance along surface to point of impingement.   Basic ellipsoid, 20 percent thick; inlet velocity ratio, 1.0.
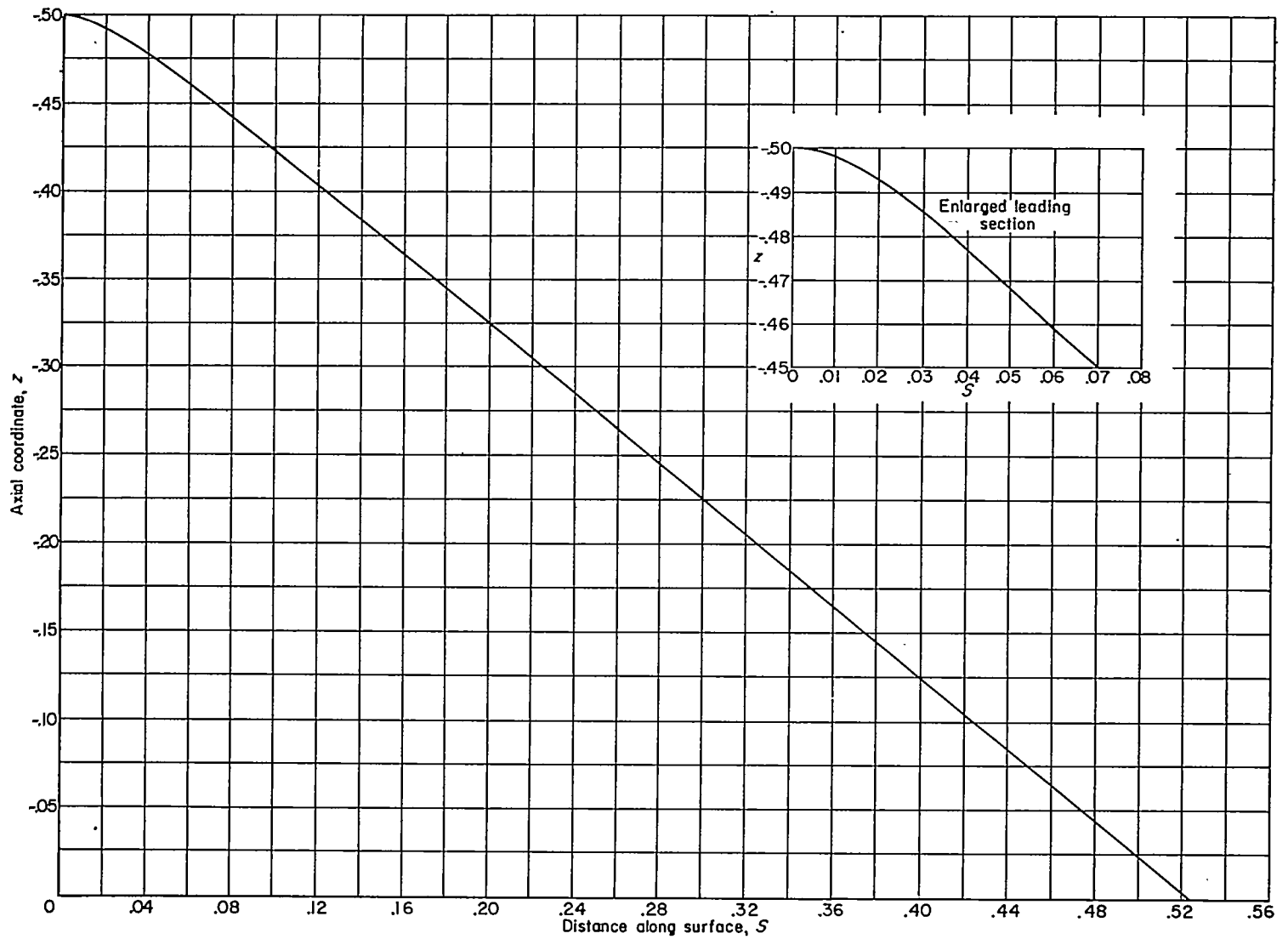
FIGURE 17.—Relation between distance along ellipsoid surface and axial coordinate.   Basic ellipsoid, 20 percent thick; inlet velocity ratio, 1.0.
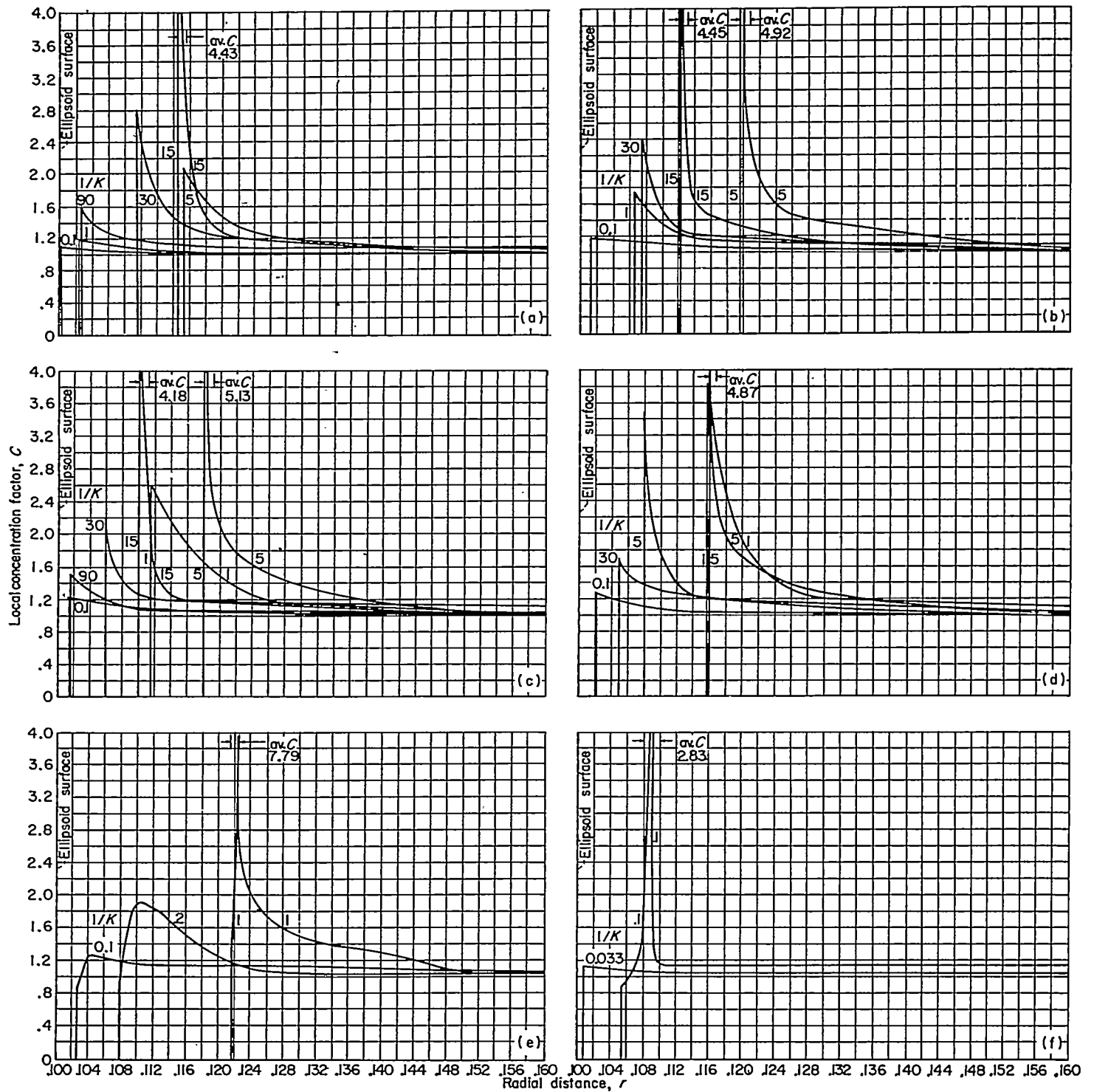
(a) $z=0$; $Re_0=0$.
(c) $z=0$; $Re_0=512$.
(e) $z=0$; $Re_0=4096$.

(b) $z=0$; $Re_0=128$.
(d) $z=0$; $Re_0=1024$.
(f) $z=0$; $Re_0=8192$.

FIGURE 18.—Variation of local concentration factor with radial distance at constant axial position.   Basic ellipsoid, 20 percent thick; inlet velocity ratio, 1.0.
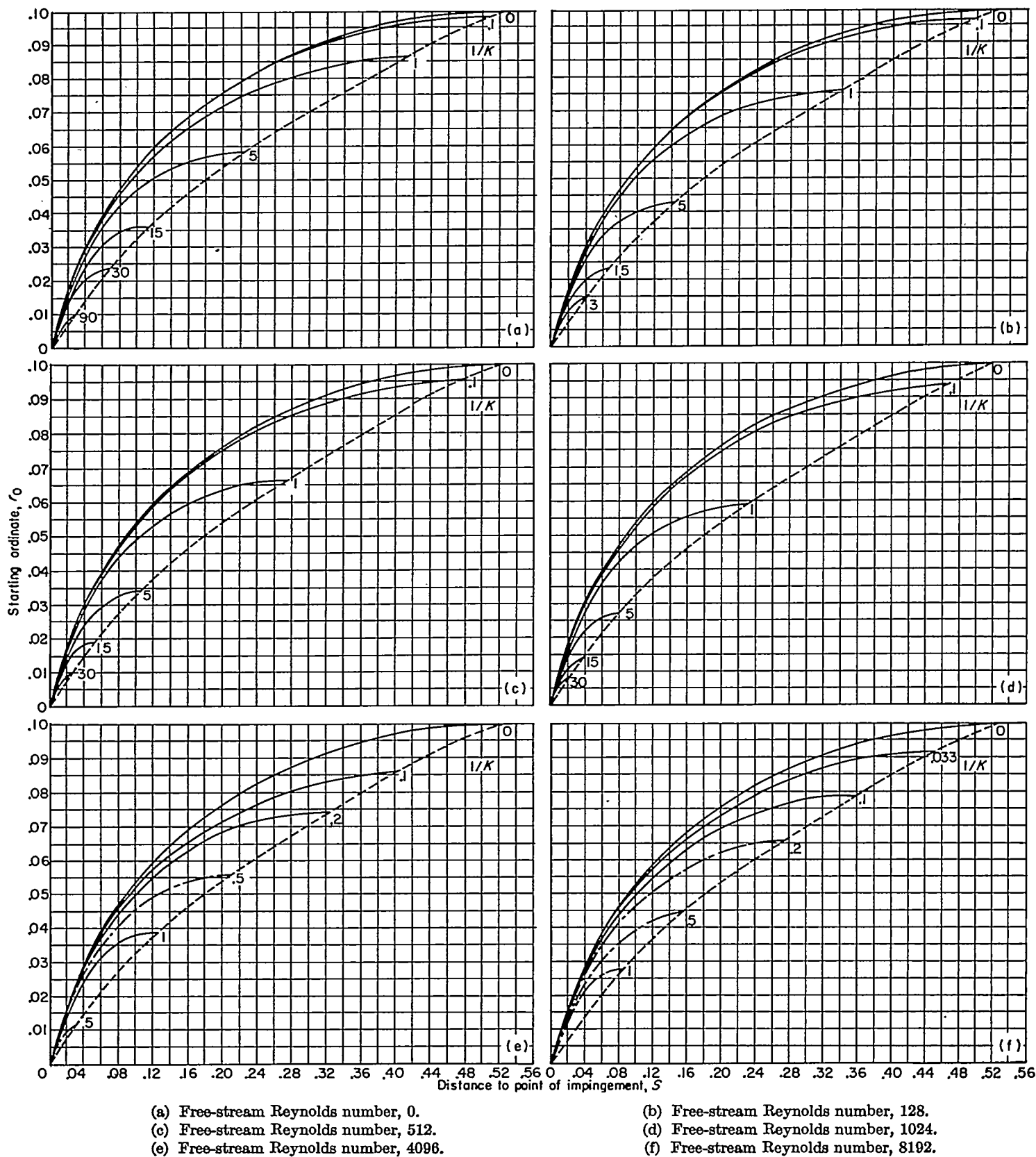
(g) $z=-0.25$; $Re_0=0$.
(i) $z=-0.25$; $Re_0=512$.
(k) $z=-0.25$; $Re_0=4096$.

(h) $z=-0.25$; $Re_0=128$.
(j) $z=-0.25$; $Re_0=1024$.
(l) $z=-0.25$; $Re_0=8192$.

FIGURE 18.—Continued.   Variation of local concentration factor with radial distance at constant axial position.   Basic ellipsoid, 20 percent thick; inlet velocity ratio, 1.0.

(m) $z=-0.50$; $Re_0=0$.

(o) $z=-0.50$; $Re_0=512$.

(q) $z=-0.50$; $Re_0=4096$.

(n) $z=-0.50$; $Re_0=128$.

(p) $z=-0.50$; $Re_0=1024$.

(r) $z=-0.50$; $Re_0=8192$.

FIGURE 18.—Concluded. Variation of local concentration factor with radial distance at constant axial position. Basic ellipsoid, 20 percent thick; inlet velocity ratio, 1.0.
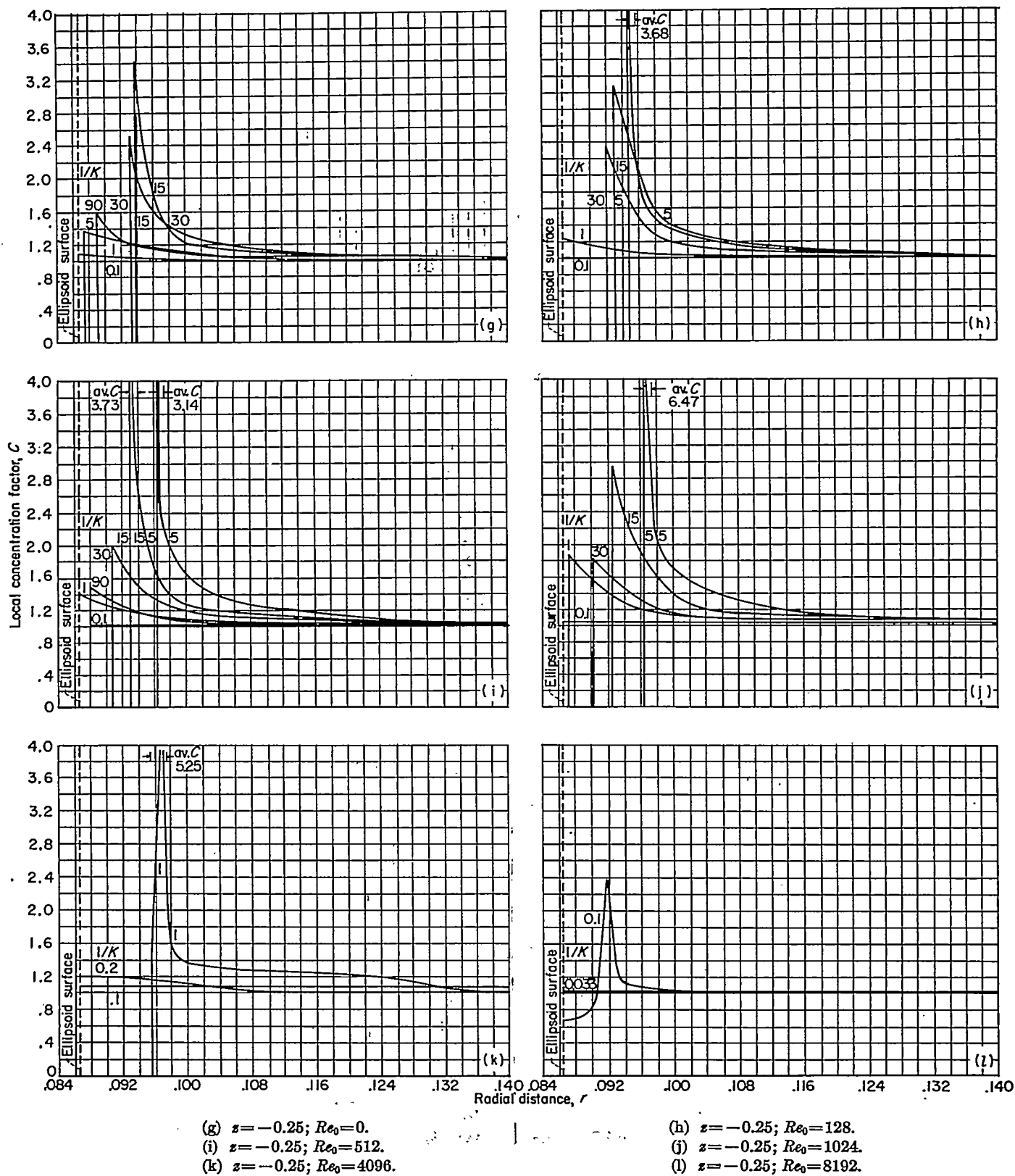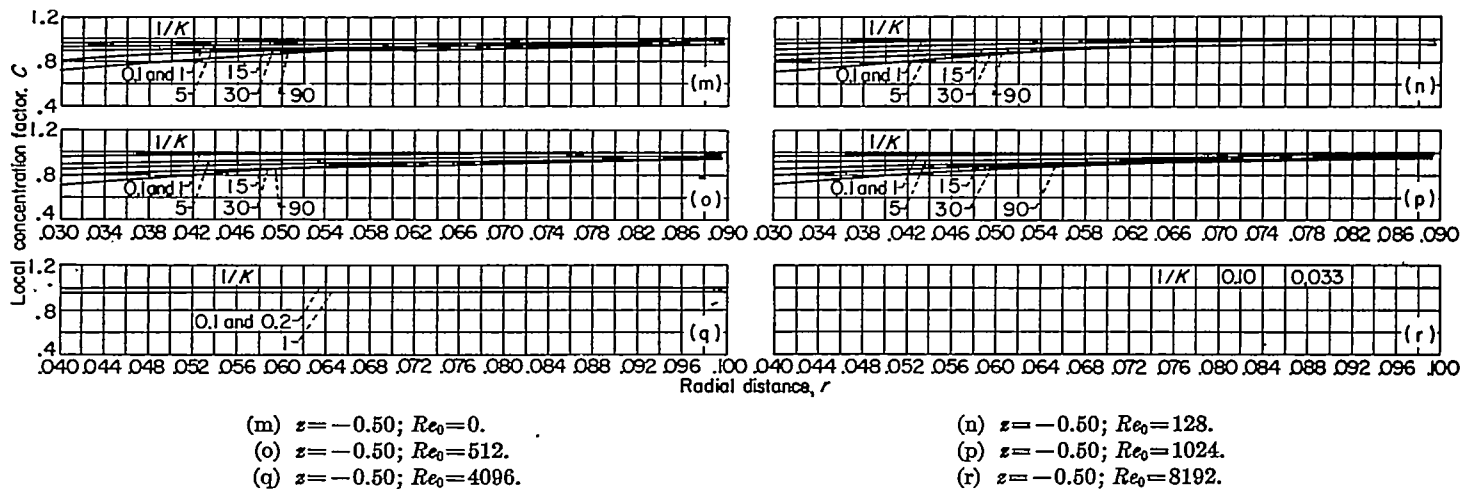
INLET WITH VELOCITY RATIO OF 0.7

The effect of changes in $1/K$ and Re_0 on droplet trajectories is illustrated in figure 19. The same range of flight and meteorological conditions covered by figure 5 is given in figure 19.

Droplet ingestion.—The amount of water in pounds per hour flowing in the region bounded by the tangent trajectory (t–t_s, fig. 4) and the upper limiting trajectory (l–l_p, fig. 4) is given by the expression

$$W_t=0.33w_0UAC_t \tag{12}$$

The derivation of this equation is based on the law of conservation of matter.

The total concentration factor C_t may be considered an ingestion efficiency (scooping ratio), since it is the ratio of the area at $z=-\infty$ between the tangent and upper limiting trajectories to the area at the inlet opening. The term C_t is defined as

$$C_t=\frac{r_{0,l}^2-r_{0,tan}^2}{(0.0714)^2-(0.04)^2} \tag{13}$$

where $r_{0,l}$ is the ordinate at $z=-\infty$ of the upper limiting trajectory, and $r_{0,tan}$ is the ordinate at infinity of the tangent trajectory. The values in the denominator are the values of r of the inner wall and cowl at the opening (points B and D, fig. 1(b)). This definition of the total concentration assumes that the area of interest A, in square feet, is a sector of an annulus with the area perpendicular to the major axis of the ellipsoid. The values of C_t are given in figure 20.

The values $r_{0,l}$ of the upper limiting trajectories and $r_{0,tan}$

of the tangent trajectories are given in figure 21. The trajectories near the body deviate more from a straight line than those near the lip of the entrance (see fig. 19); therefore the ordinates at $z=-\infty$ of the upper limiting trajectories are not affected by changes in Re_0 and $1/K$ so much as the tangent trajectories.

Variation of liquid water across inlet opening.—The local weight flux of water in droplet form is obtained from equation (11). The local concentration factor C at a point r in space at $z=-0.30$ and -0.25 is obtained from figure 22. The largest values of concentration factor are near the forebody, just above the shadow zone. The variation in local concentration radially across the inlet is very similar to the spatial variation for the inlet with a velocity ratio of 1.0 (figs. 11 and 18).
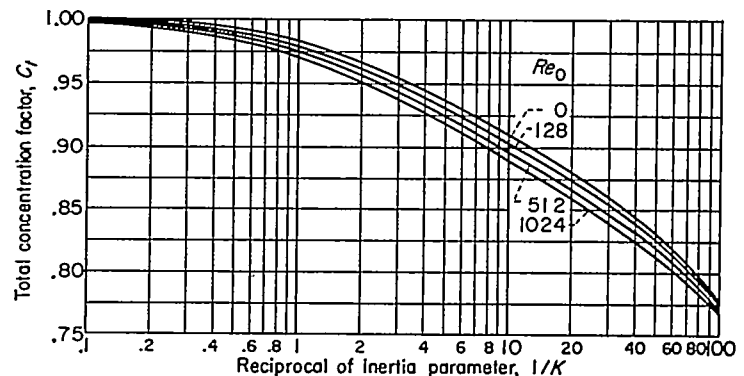

FIGURE 20.—Total concentration factor as function of free-stream Reynolds number and reciprocal of inertia parameter. Inlet velocity ratio, 0.7.
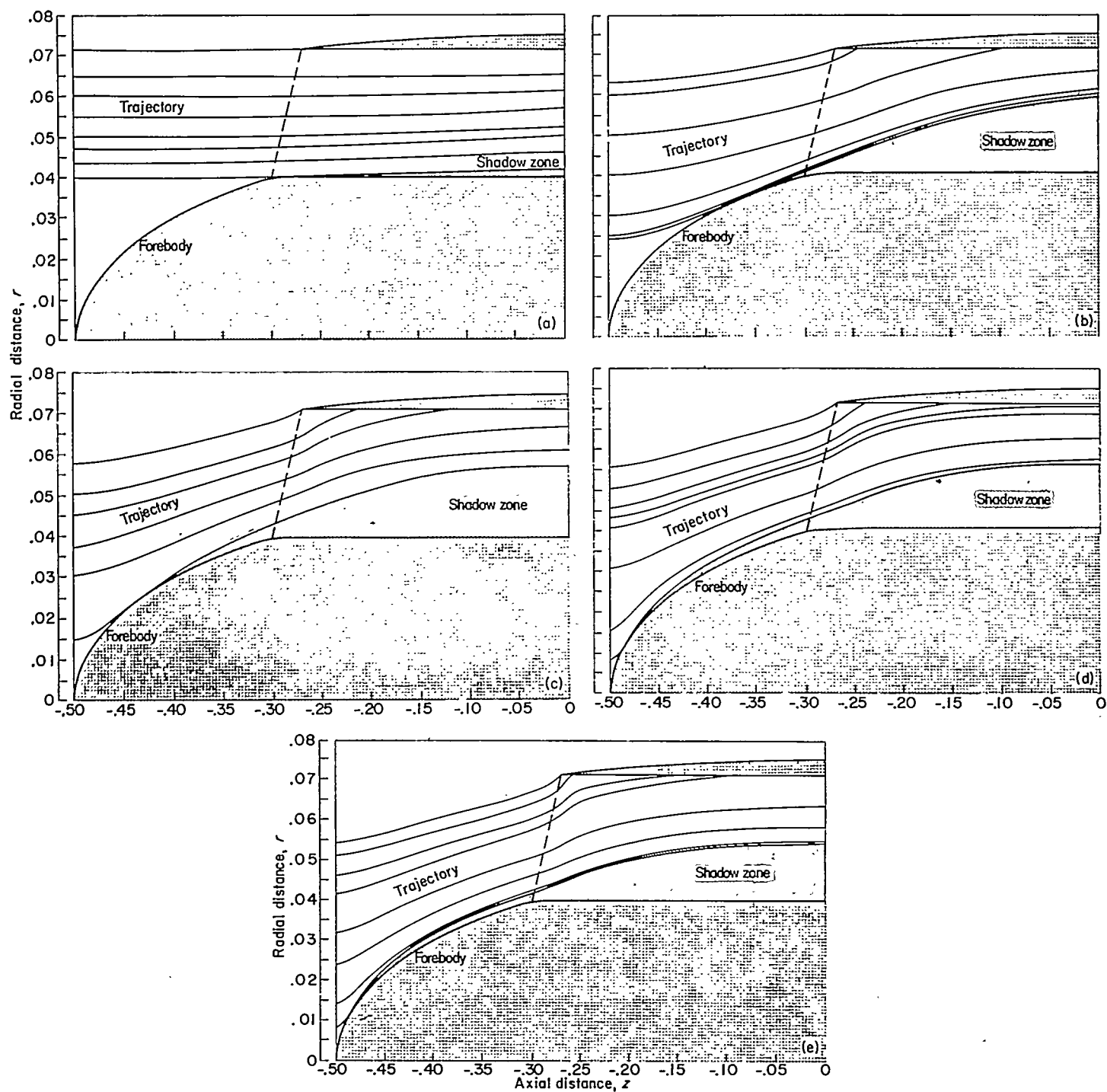
(a) $1/K=1/30$; $Re_0=8192$.
(c) $1/K=15$; $Re_0=128$.

(b) $1/K=3$; $Re_0=512$.
(d) $1/K=45$; $Re_0=128$.

(e) $1/K=114$; $Re_0=8$.

FIGURE 19.—Trajectories for inlet with velocity ratio of 0.7.
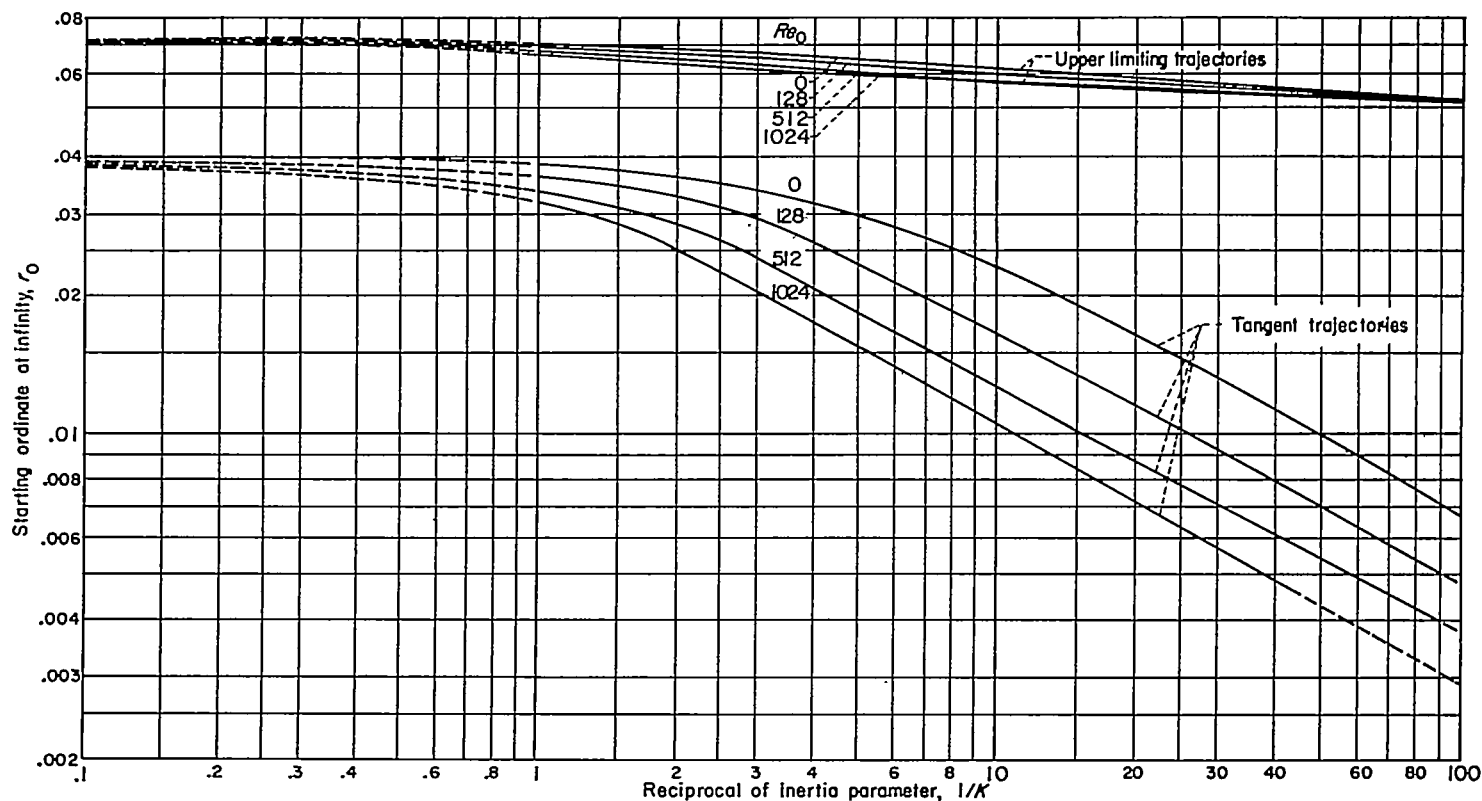
FIGURE 21.—Starting ordinates of upper limiting trajectories and tangent trajectories.   Inlet velocity ratio, 0.7.

Shadow zone.—A region of zero concentration exists adjacent to the surface of the inner wall. The thickness $(r-r_s)$ of this shadow zone at each z-position on the body for various values of Re_0 and $1/K$ is given in figure 23. The magnitude of the shadow zone depends on both Re_0 and $1/K$, as in the preceding case of the inlet with a velocity ratio of 1.0. For the inlet with a velocity ratio of 0.7, the thickness of the shadow zone becomes appreciable inside the inlet, because the inner wall becomes a straight line parallel to the major axis.

Total impingement on cowl.—Although the wall thickness does not appreciably affect the total water ingested, the wall shape is important in determining impingement on the wall. With the particular value of inlet velocity ratio studied (0.7), no impingement occurs on the outer surface of the cowl for values of $1/K$ larger than 1. This means that for most flight and atmospheric conditions (see table I) only large drops will impinge on the outer surface of the cowl.

(a) $z=-0.30$; $1/K=1$.
(b) $z=-0.30$; $1/K=3$.
(c) $z=-0.30$; $1/K=15$.

(d) $z=-0.30$; $1/K=45$.
(e) $z=-0.30$; $1/K=90$.
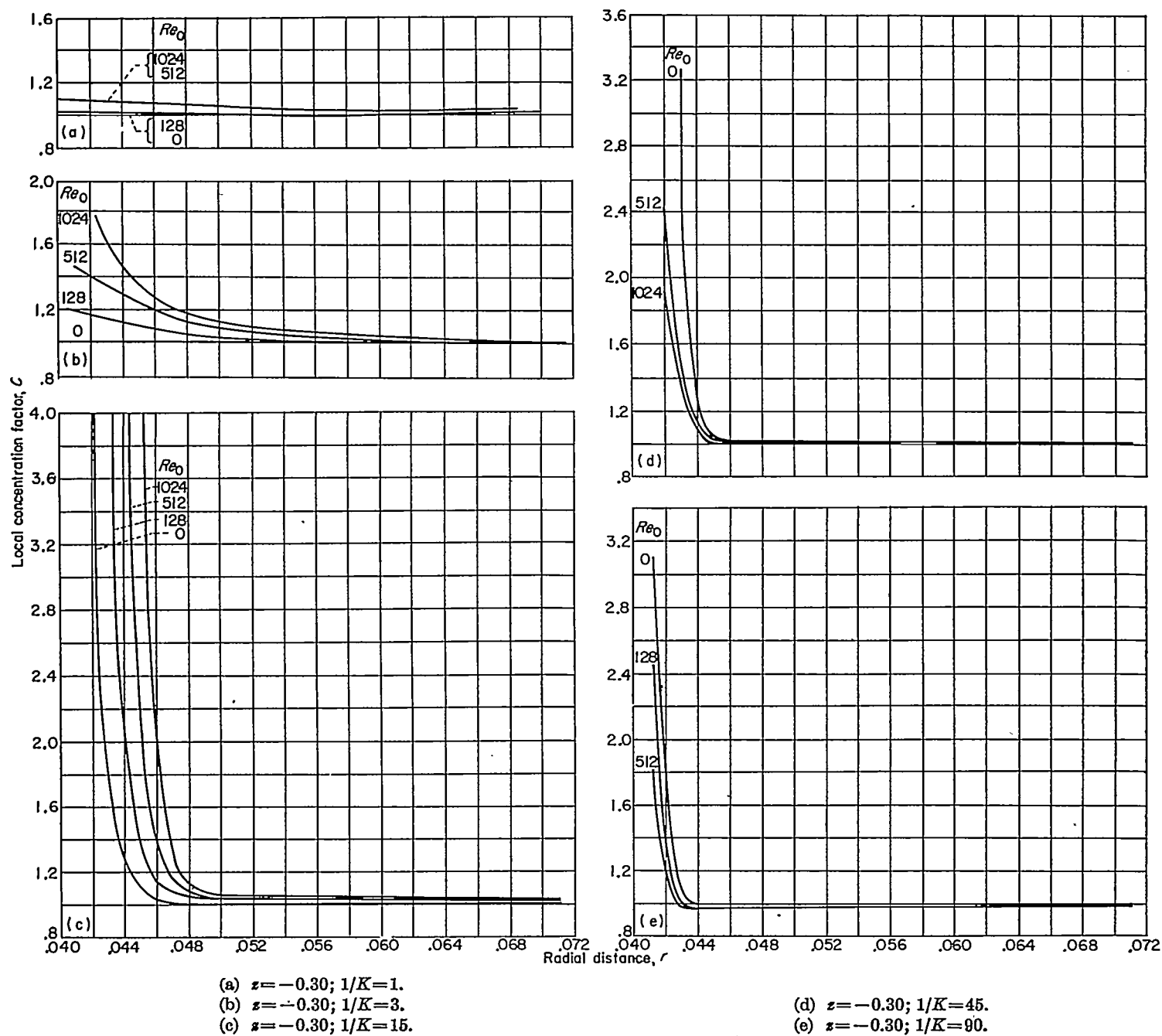
FIGURE 22.—Local concentration factor as function of radial distance of inlet opening.   Inlet velocity ratio, 0.7.

(f) $z=-0.25$; $1/K=1$.
(g) $z=-0.25$; $1/K=3$.
(h) $z=-0.25$; $1/K=15$.

(i) $z=-0.25$; $1/K=45$.
(j) $z=-0.25$; $1/K=90$.
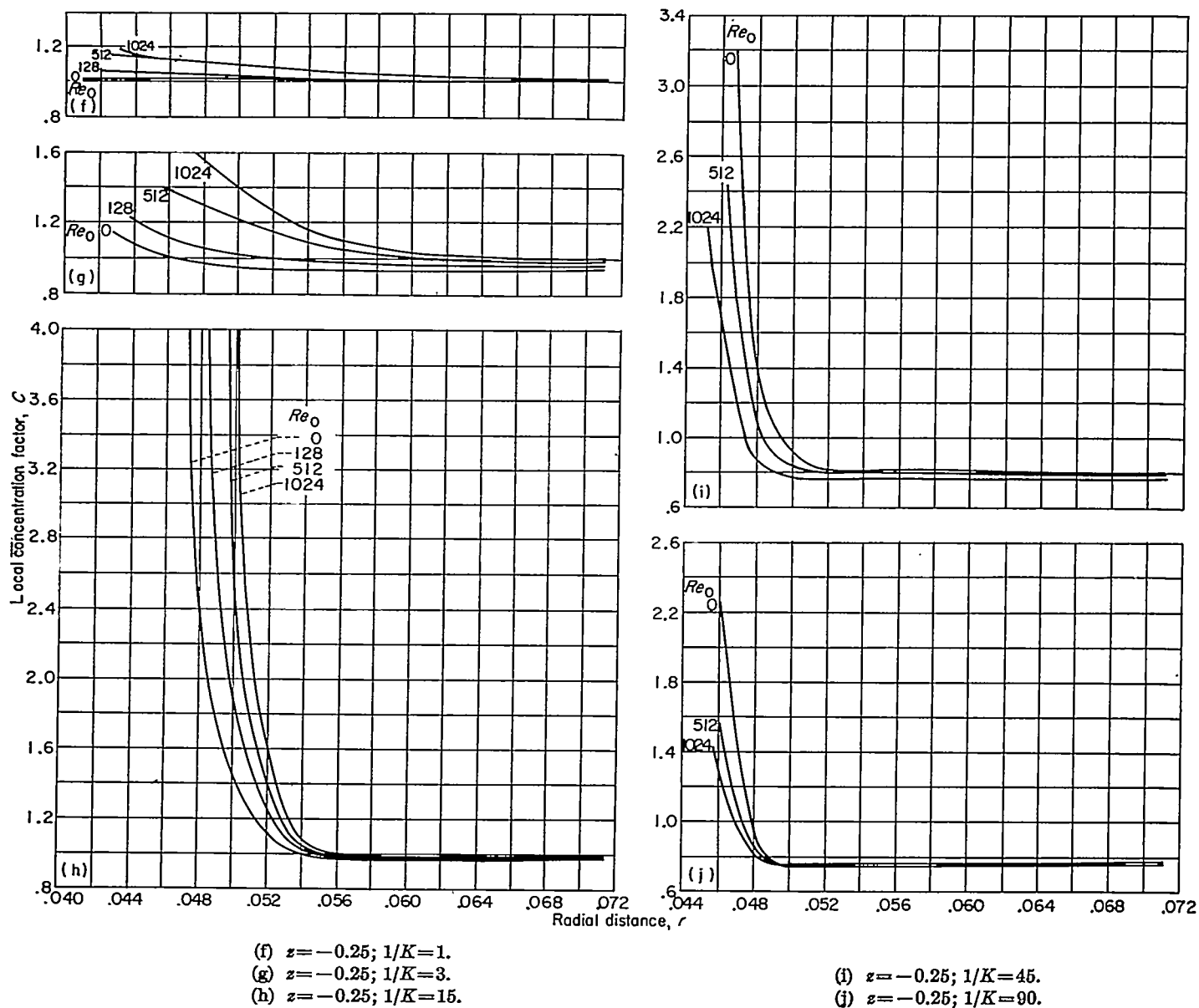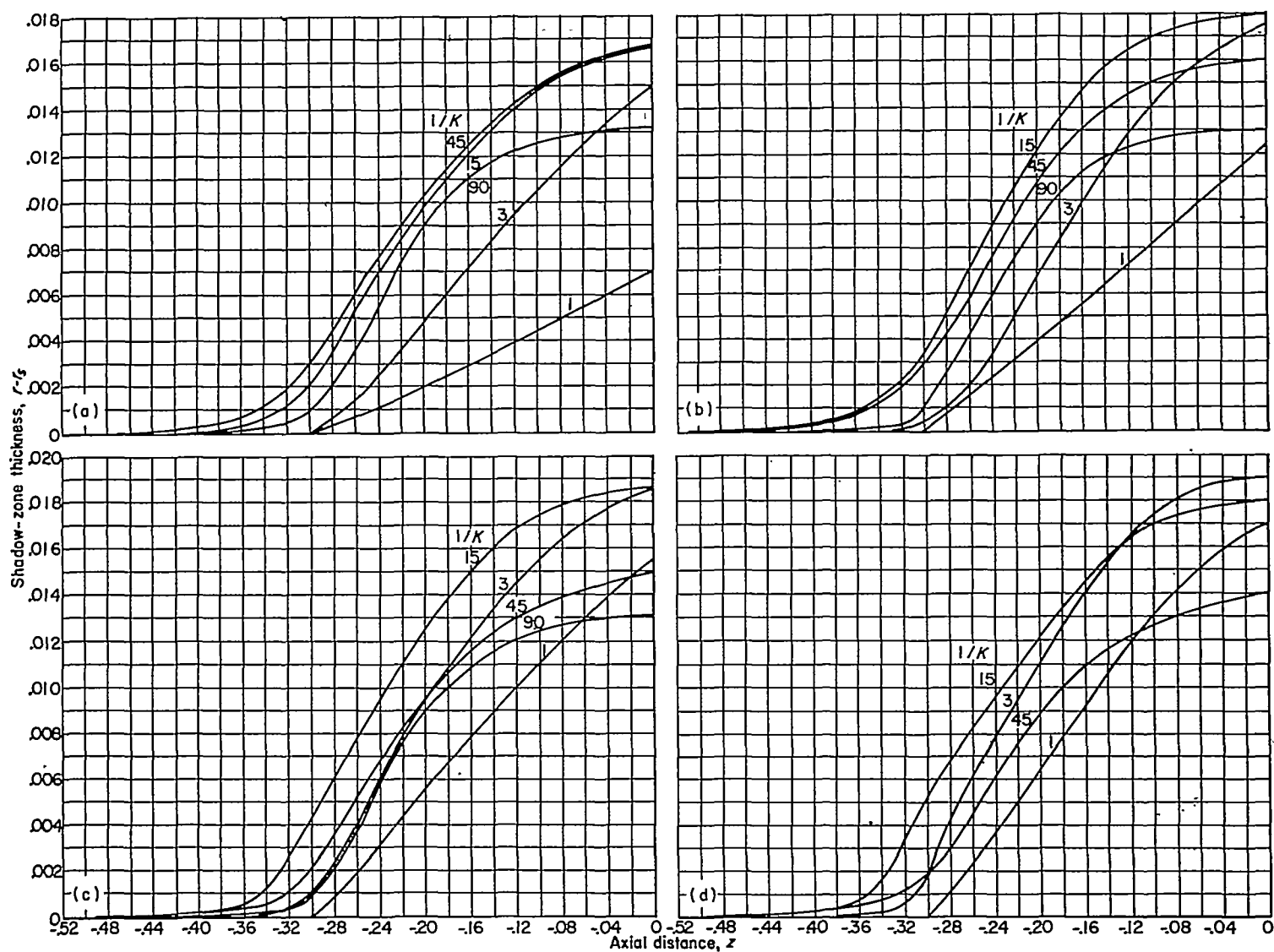
FIGURE 22.—Concluded.   Local concentration factor as function of radial distance of inlet opening.   Inlet velocity ratio, 0.7.

(a) Free-stream Reynolds number, 0.
(c) Free-stream Reynolds number, 512.

(b) Free-stream Reynolds number, 128.
(d) Free-stream Reynolds number, 1024.

FIGURE 23.—Thickness of shadow zone along inlet inner wall.   Inlet velocity ratio, 0.7; angle of attack, 0°.
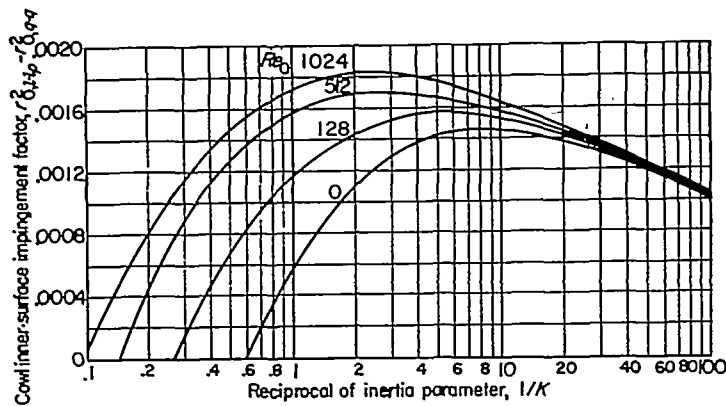
FIGURE 24.—Cowl inner-surface impingement factor. Inlet velocity ratio, 0.7.

The amount of water in droplet form impinging on the inner surface of the cowl is

$$W_c = 0.33\pi w_0 U L^2 (r^2_{0,L-l_p} - r^2_{0,q-q}) \qquad (14)$$

The values of $(r^2_{0,L-l_p} - r^2_{0,q-q})$ required in equation (14) are given in figure 24. The impingement study is confined to the surface between points D and F (fig. 4), because trajectories were not calculated beyond the midsection of the ellipsoid ($z=0$).

Impingement distribution on cowl.—The rate of water impingement per unit area on the inner surface of the cowl

between points D and F (fig. 4) can be found by applying the values of β_c given in figure 25 to

$$W_{\beta,c} = 2.3 w_0 U \beta_c \qquad (15)$$

This equation is derived from the concept that the flux of water in droplet form through an annular area of space width $r_2 - r_1$ impinges on the cowl surface between points $S_{c,2}$ and $S_{c,1}$:

$$W_{\beta,c} = 0.33 \ w_0 U \ \frac{\pi (r^2_2 - r^2_1)_0}{2\pi (0.0714)(S_2 - S_1)_c} = 2.3 \ w_0 U \ \frac{\Delta r^2_0}{\Delta S_c}$$

where, in the differential limit,

$$\frac{dr^2_0}{dS_c} = \beta_c$$

The local impingement factors β_c are given in figure 25 as functions of the surface distance S_c, starting from the inlet lip at point D. For all values of $1/K$ and Re_0 the maximum impingement rate occurs at the entrance lip. Although the high rate occurs between the entrance lip and approximately $S_c = 0.02$ (ratio of actual distance to major axis), the remainder of the surface is exposed to impingement. The impingement distribution on the inner surface of the cowl is obtained directly from figure 25, because $W_{\beta,c}$ is directly proportional to β_c (eq. (15)). The integral of $W_{\beta,c}$ between the cowl lip and $z=0$ is equal to the total impingement on the cowl W_c given in the preceding section.
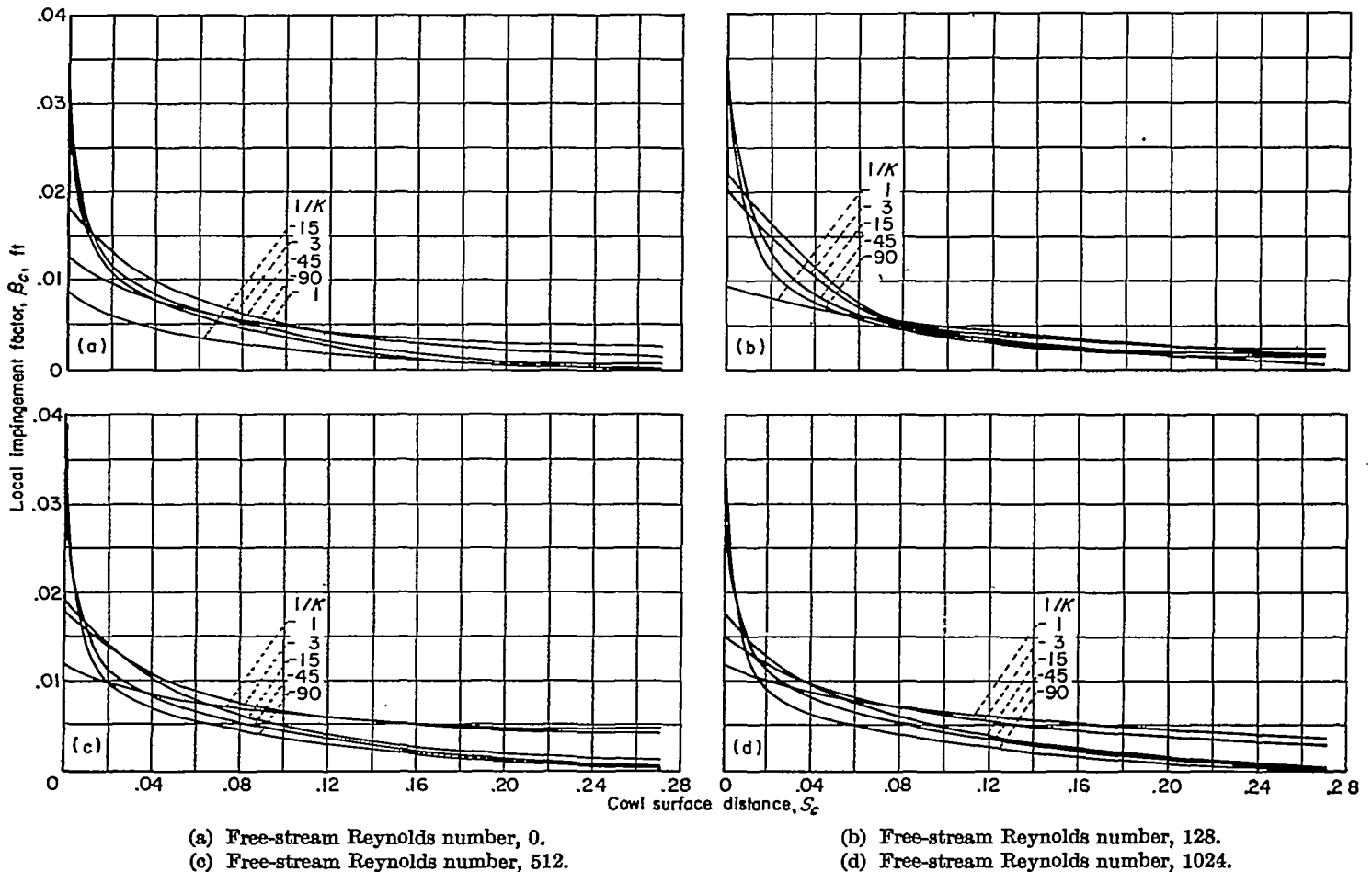
(a) Free-stream Reynolds number, 0.
(c) Free-stream Reynolds number, 512.

(b) Free-stream Reynolds number, 128.
(d) Free-stream Reynolds number, 1024.

FIGURE 25.—Local collection efficiency as function of surface distance. Inlet velocity ratio, 0.7.

COMPARISON OF INLETS WITH VELOCITY RATIOS 1.0 AND 0.7

The two types of entrances discussed herein can be compared in a limited manner only. The configuration with the inlet velocity ratio of 1.0 and 10-percent-thick basic ellipsoid must be confined to that configuration which most nearly corresponds to the fixed geometric shape of the 0.7-velocity-ratio inlet. An air streamline (line DE, fig. 3) exists for the inlet with a velocity ratio of 1.0 that superposes very well on the wall DE (fig. 4) of the 0.7-velocity-ratio inlet. An inlet composed of elliptical forebody ABC and cowl DE, shown in figure 3, is compared with an inlet configuration shown in figure 4. The corresponding configurations are also shown in figures 1(a) and (b), respectively.

The principal geometric difference in the two configurations is that the cowl DE in figure 3 (also fig. 1(a)) has negligible thickness; whereas, the cowl in figure 4 (also fig. 1(b)) has thickness EF at $z=0$. In spite of the thickness EF, the cowl of the 0.7-velocity-ratio inlet is very thin, approximating a thin wedge (in sectional view) with a sharp edge at the entrance point D. The relative geometric proportions of the 0.7-velocity-ratio inlet are best illustrated in figure 1(b). (As was previously stated, the ordinate scale in fig. 4 is expanded with respect to the abscissa scale.) The wall is not thick enough to be of consequence in the influencing of the airflow field ahead of the inlet. The inlet inner walls are also shaped somewhat differently; the inlet opening areas are the same and in both inlets remain approximately constant from the opening through to $z=0$. In spite of the small differences mentioned, the two inlet configurations are enough alike to permit comparison of the total water ingested and the distribution on the cowl inner surface for the two velocity ratios.

TOTAL WATER INGESTED

In order to facilitate the presentation of results, the comparison is made at several specific flight and atmospheric conditions. The conditions chosen are the same as those represented by the trajectories of figures 5 and 19. These conditions are representaive of a wide range of values of $1/K$ and Re_0. However, a danger must be noted arising from the choice of only a few sets of conditions for comparison: The relative importance of the different factors being compared, such as flight speed, droplet diameter, and so forth, may change when other numerical values are chosen.

The comparative results are presented in the following tabulation as ingestion efficiencies. The ingestion efficiency (or scooping ratio) is the ratio of the water ingested to the total water in an annular space with a cross-sectional area equal to that of the inlet and a volume in free space equal to that swept out by the inlet.

The ingestion efficiency includes the water that impinges on the inner wall. For $1/K=1/30$, $Re_0=8192$, and a 1.0-velocity-ratio inlet, 8 percent of the water passing through the opening strikes the inner wall (impinges on ellipsoid surface beyond the opening). For all other conditions tabulated, all or almost all the water ingested does not strike the inside surface of the cowl up to the midsection ($z=0$). For $1/K=3$, $Re_0=512$, and a 1.0-velocity-ratio inlet, a slight concentration effect is present, which results in an ingestion efficiency of 102 percent. The ingestion efficiency of the inlet with a velocity ratio of 1.0 is over 90 percent and less than 104 percent for a wide range of conditions listed in table I.

The ingestion efficiency of the inlet with a velocity ratio of 0.7 is always over 75 percent and never over 100 percent for the conditions listed in table I. The ingestion efficiency for this inlet is found directly from figure 20, which presents the total concentration factor. Ingestion efficiency is 100 times larger than the C_t factor of figure 20. For comparable flight and atmospheric conditions, somewhat less water is ingested at 0.7 velocity ratio than at 1.0, except for rain drops.

DISTRIBUTION OF WATER ON INNER SURFACE OF COWL

A detailed quantitative comparison of the water distribution has little practical application, because small changes in shape of the walls affect the distribution appreciably. A reasonable qualitative comparison can be made easily by examining figures 5 and 19; for example, for $1/K=1/30$ and $Re_0=8192$ (figs. 5(a) and 19(a)), the trajectories for both inlets are practically straight lines, with consequent slight impingement on the outer surface and no impingement on the inner surface of the cowl. For other combinations of $1/K$ and Re_0 in figures 5(b) to (e) and 19(b) to (e), in which there is some impingement on the inner surface of the cowl for both inlets, the distribution of this impingement differs between the two inlets. For the inlet with a velocity ratio of 1.0, the trajectories are nearly parallel to the cowl (located at DE, fig. 3). The small amount of impingement is spread fairly evenly from points D to E of the wall surface. For the inlet with a velocity ratio of 0.7, the distribution is much higher near the inlet opening (see fig. 25 for values of local impingement factors). Thus, lowering inlet velocity ratio from 1.0 to 0.7 tends to distribute the impingement less evenly on the inner surface of the cowl with greater concentration near the opening.

For both inlets in an actual cloud in which a distribution of droplet sizes is present, the area some distance beyond the lip (say $S_c>0.1$) can be expected to build up unevenly with ice if this area is unprotected. The reason for this expected jaggedness in the ice buildup is that the droplets strike the wall surface at a small angle (trajectories nearly parallel to surface, see figs. 5 and 19). The points of impingement of the small droplets in the cloud are influenced by small irregularities of the wall surface and by small-scale turbulence near the wall. The start of ice buildup at a point of

Flight speed, mph	Pressure altitude, ft	Droplet diam., d, microns	Ellipsoid major axis, L, ft	Reciprocal of inertia parameter, $1/K$	Free-stream Reynolds number, Re_0	Ingestion efficiency, percent	
						1.0-Velocity-ratio inlet	0.7-Velocity-ratio inlet
300	5,000	1000	50	1/30	8192	100	100
	15,000	80	29	3	512	102	94
		20	10	15	128	99	89
		27	27	45	128	97	83
50	25,000	10	3	114	8	94	78

wall irregularity produces an unstable condition that promotes further growth of ice on that particular point and produces further turbulence for other growths.

SHADOW ZONE

The shadow zone is increased considerably in the 0.7-velocity-ratio inlet as compared with the 1.0-velocity-ratio inlet, principally because of the change in physical geometry of the inner wall rather than the change in velocity ratio. The shapes of the tangent trajectories, which determine one boundary of the shadow zone, are very similar in the two inlets for comparable flight and atmospheric conditions.

In both inlets and for some flight and atmospheric conditions the thickness of the shadow zone becomes appreciable inside the inlet. If possible, consideration of the shadow zone should be given in the positioning of boundary-layer scoops. The thickness presented in figures 6, 13, and 23 is for 0° angle of attack. A boundary-layer scoop designed according to these figures to be in the shadow zone might be subjected to heavy concentration when the aircraft is yawed or pitched, because the thickness of the shadow zone is very sensitive to changes in angle of attack.

CONCLUDING REMARKS

The data presented herein can be used as a guide in the evaluation of water ingestion in inlets. The studies on the simple shapes at 0° angle of attack lead to some general concepts of water ingestion in inlets. The amount of water ingested is not sensitive to small changes in shape of the outer wall. The placement of a wall in the airflow will usually disturb the airflow more than the droplet trajectories. The impingement on the cowl (i. e., amount and distribution) is quite sensitive to the physical shape and surface condition of the wall. In most applications impingement on the interior surface of the cowl can be expected for a considerable distance inside the entrance, because the forebody deviates the trajectories away from the body and toward the cowl.

The use of screens and boundary-layer-removal scoops at the entrance requires careful design because of the existence of the shadow zone and regions of high concentration. The variation in concentration of water across an inlet shows that a screen can build up ice unevenly in such manner as to result in large radial-flow distortions.

Although only one inlet configuration was studied at an inlet velocity ratio of 0.7, the general concept that lowering the inlet velocity ratio lowers the ingestion efficiency can be applied to a large variety of configurations. This concept is evident from a study of the manner in which air streamlines change when the inlet-air velocity ratio is decreased for a particular configuration. Since most aircraft (particularly interceptor types) should be designed with protection against ice formations during loitering, climb, and letdown, a design based on water-ingestion data for an inlet velocity ratio of 1.0 will be adequate for lower velocity ratios. A lowering of the velocity ratio will also result in higher impingement near the inlet opening on the inner surface of the cowl.

As can be seen from figures 5 and 19, no impingement occurs on the outer surface of the cowl over a large range of meteorological and flight conditions. High local impingement efficiencies can be expected on the cowl lip for all entrance velocity ratios.

During the major portion of most flight plans the inlet velocity ratio does not exceed 1.0 and does not decrease below 0.7. For most inlet designs, the accuracy of the methods presented herein for estimating amount and distribution of impingement is within the accuracy of knowledge of the meteorological factors involved, such as liquid-water content and droplet size.

As was stated early in this report, droplets that impinge on the forebody are assumed to be removed from the possibility of entering the inlets. In reality, the water deposited on the forebody may run back over the body surface and into the inlet when the ice is melted by thermal anti-icing devices. A discussion of runback is beyond the scope of this report. The conditions resulting in runback and the effect of runback on screens, boundary-layer scoops, and other devices in the inlets should be carefully considered in inlet designs.

Although the calculations were made for incompressible flow, they should be applicable throughout the subsonic region because of the small effect of compressibility on droplet trajectories (ref. 5) and the high flight critical Mach number of the configurations studied.

LEWIS FLIGHT PROPULSION LABORATORY
    NATIONAL ADVISORY COMMITTEE FOR AERONAUTICS
        CLEVELAND, OHIO, *November 2, 1955*

APPENDIX A

SYMBOLS

A area; sector of annulus in plane perpendicular to major axis, sq ft

a droplet radius, ft

C local concentration factor, dimensionless

C_D coefficient of drag, dimensionless

C_t total concentration factor, dimensionless

c,g constants for size of inlet (see eq. (2))

d droplet diameter, microns

F weight flux of water, lb/(hr)(sq ft)

K inertia parameter, dimensionless

L major axis of ellipse, ft

Re local Reynolds number with respect to droplet, dimensionless

Re_0 free-stream Reynolds number with respect to droplet, dimensionless

r,z cylindrical coordinates, ratio of actual length to major axis, dimensionless

S distance along surface of ellipsoid measured from stagnation point, ratio of actual distance to major axis, dimensionless

S_c distance along inner surface of cowl measured from point of inlet opening, ratio of actual distance to major axis, dimensionless

t time, sec

U free-stream airspeed, mph

U^* free-stream airspeed, ft/sec

u local air velocity, ratio to free-stream velocity, dimensionless

v local droplet velocity, ratio to free-stream velocity, dimensionless

W_{B-t_s} rate of water impingement on inner wall, lb/hr

W_c rate of water impingement on cowl, lb/hr

W_i rate of water ingestion, lb/hr

$W_{\beta,c}$ local rate of water impingement on surface of cowl, lb/(hr)(sq ft)

w liquid-water content in cloud, g/cu m

α ¼ focal distance of ellipsoid

β_c local impingement factor on cowl, ft

ϵ eccentricity of ellipse defined by a meridian section of ellipsoid of revolution

λ,μ_1 prolate-elliptic coordinates

μ viscosity of air, slugs/(ft)(sec)

ρ density, slugs/cu ft

τ dimensionless time function, $\tau=tU^*/L$

φ potential function

ψ streamline function

Subscripts:

a air

B point of inlet entrance on ellipsoid surface

l lip

r radial component

s shadow

tan tangent

w water

z axial component

0 free-stream conditions

APPENDIX B

DERIVATION OF PERTURBATION FIELD FOR 0.7-VELOCITY-RATIO INLET

The airflow field for configuration 2 (fig. 1(b)) was obtained by adding a two-dimensional perturbation field to the basic flow field about a 10-percent-thick ellipsoid of revolution. The perturbation field had the configuration described in reference 9 and mentioned in reference 10 under the name "Borda mouthpiece." This perturbation field is expressed by the complex function

$$\zeta^* = \theta^* + e^{\theta^*} \tag{B1}$$

where

$$\zeta^* = z^* + ir^* \tag{B2}$$

$$\theta^* = \varphi + i\psi \tag{B3}$$

and the asterisk denotes special coordinates applicable only to the Borda mouthpiece and differing from those of the basic ellipsoid.

The rectangular coordinates are given parametrically by

$$z^* = \varphi + e^{\varphi} \cos \psi \tag{B4}$$

$$r^* = \psi + e^{\varphi} \sin \psi \tag{B5}$$

The application of the Cauchy-Riemann conditions

$$u_z^* = \frac{\partial \varphi}{\partial z^*} = \frac{\partial \psi}{\partial r^*}$$

$$u_r^* = \frac{\partial \varphi}{\partial r^*} = -\frac{\partial \psi}{\partial z^*}$$

results in the velocity components:

$$u_z^* = \frac{1 + e^{\varphi} \cos \psi}{1 + 2e^{\varphi} \cos \psi + e^{2\varphi}} \tag{B6}$$

$$u_r^* = \frac{e^{\varphi} \sin \psi}{1 + 2e^{\varphi} \cos \psi + e^{2\varphi}} \tag{B7}$$

In order to give the inlet proper position and size with respect to the basic ellipsoid, it is necessary to perform a translation and change of scale according to the following transformation:

$$z = 0.00943z^* + 0.2780 = 0.00943(\varphi + e^{\varphi} \cos \psi) + 0.2780 \tag{B8}$$

$$r = 0.00943r^* + 0.0418 = 0.00943(\psi + e^{\varphi} \sin \psi) + 0.0418 \tag{B9}$$

A z,r point described by these equations corresponds to the same point in space described by the z,r coordinates used for the basic ellipsoid. The transformation leaves the velocity components unchanged; but, for an inlet velocity ratio of 0.7, they must be expressed in terms of the free-stream velocity U and inlet velocity u as

$$u_{z,p} = \frac{1 + e^{\varphi} \cos \psi}{1 + 2e^{\varphi} \cos \psi + e^{2\varphi}} \left(1 - \frac{u}{U}\right) = \frac{0.3(1 + e^{\varphi} \cos \psi)}{1 + 2e^{\varphi} \cos \psi + e^{2\varphi}} \tag{B10}$$

$$u_{r,p} = \frac{e^{\varphi} \sin \psi}{1 + 2e^{\varphi} \cos \psi + e^{2\varphi}} \left(1 - \frac{u}{U}\right) = \frac{0.3e^{\varphi} \sin \psi}{1 + 2e^{\varphi} \cos \psi + e^{2\varphi}} \tag{B11}$$

where the subscript p denotes the perturbation to be added to the field about the ellipsoid.

The transformation given in the equations (B8) and (B9) approximately matches one streamline of the perturbation field to the surface of the basic ellipsoid. Adding the perturbation velocity components in equations (B10) and (B11) to the velocity components of the basic 10-percent-thick ellipsoid gives one streamline that is the forebody ABC shown in figure 1(b) and another streamline that is the inlet outer wall FDE. Also, when the perturbation velocities obtained from equations (B10) and (B11) are added to the basic components, the resulting velocity at the center of the inlet opening is 0.714 with respect to the free-stream velocity U, but 0.7 with respect to the local basic-ellipsoid velocity.

The velocity components of the basic flow field may be obtained from equations given in reference 1 and plotted in figure 2 of reference 3.

REFERENCES

1. Dorsch, Robert G., Brun, Rinaldo J., and Gregg, John L.: Impingement of Water Droplets on an Ellipsoid with Fineness Ratio 5 in Axisymmetric Flow. NACA TN 3099, 1954.
2. Dorsch, Robert G., and Brun, Rinaldo J.: Variation of Local Liquid-Water Concentration About an Ellipsoid of Fineness Ratio 5 Moving in a Droplet Field. NACA TN 3153, 1954.
3. Brun, Rinaldo J., and Dorsch, Robert G.: Impingement of Water Droplets on an Ellipsoid with Fineness Ratio 10 in Axisymmetric Flow. NACA TN 3147, 1954.
4. Brun, Rinaldo J., and Dorsch, Robert G.: Variation of Local Liquid-Water Concentration About an Ellipsoid of Fineness Ratio 10 Moving in a Droplet Field. NACA TN 3410, 1955.
5. Brun, R. J., Lewis, W., Perkins, P. J., and Serafini, J. S.: Impingement of Cloud Droplets on a Cylinder and Procedure for Measuring Liquid-Water Content and Droplet Sizes in Supercooled Clouds by Rotating Multicylinder Method. NACA Rep. 1215, 1955. (Supersedes NACA TN's 2903, 2904, and NACA RM E53D23.)
6. Brun, Rinaldo J., and Mergler, Harry W.: Impingement of Water Droplets on a Cylinder in an Incompressible Flow Field and Evaluation of Rotating Multicylinder Method for Measurement of Droplet-Size Distribution, Volume-Median Droplet Size, and Liquid-Water Content in Clouds. NACA TN 2904, 1953.
7. Langmuir, Irving, and Blodgett, Katherine B.: A Mathematical Investigation of Water Droplet Trajectories. Tech. Rep. No. 5418, Air Materiel Command, AAF, Feb. 19, 1946. (Contract No. W-33-038-ac-9151 with General Electric Co.)
8. Brun, Rinaldo J., Gallagher, Helen M., and Vogt, Dorothea E.: Impingement of Water Droplets on NACA 65₁-208 and 65₁-212 Airfoils at 4° Angle of Attack. NACA TN 2952, 1953.
9. Lamb, Horace: Hydrodynamics. First Am. ed., Dover Pub., 1945.
10. Prandtl, L., and Tietjens, O. G.: Fundamentals of Hydro- and Aerodynamics. First ed., McGraw-Hill Book Co., Inc., 1934.

TABLE I.—RELATION OF DIMENSIONLESS PARAMETERS TO ELLIPSOID SIZE AND ATMOSPHERIC AND FLIGHT CONDITIONS

Atmospheric condition	Ellipsoid velocity, U, mph	Droplet diam., d, microns	Major axis, L, ft	5,000 — 20°F Re_0	5,000 — 20°F K	5,000 — 20°F $1/K$	15,000 — 1°F Re_0	15,000 — 1°F K	15,000 — 1°F $1/K$	25,000 — −25°F Re_0	25,000 — −25°F K	25,000 — −25°F $1/K$
Cloud droplets	50	10	3	14.7	0.008123	123.1	10.72	0.008383	119.3	7.836	0.008793	113.7
			30	14.7	.0008123	1231	10.72	.0008383	1193	7.836	.0008793	1137
			100	14.7	.0002437	4103	10.72	.0002515	3976	7.836	.0002638	3791
		50	3	73.54	0.2031	4.924	53.62	0.2096	4.771	39.17	0.2198	4.550
			30	73.54	.02031	49.24	53.62	.02096	47.71	39.17	.02198	45.50
			100	73.54	.006092	164.1	53.62	.006289	159.0	39.17	.006594	151.7
	100	20	10	58.81	0.01949	51.31	42.89	0.02012	49.70	31.34	0.02110	47.39
			50	58.81	.003898	256.5	42.89	.004024	248.5	31.34	.00422	237.0
			300	58.81	.0006497	1539	42.89	.0006707	1491	31.34	.0007033	1422
	300	20	10	176.4	0.05846	17.11	128.7	0.06037	16.56	94.00	0.06330	15.8
			50	176.4	.01169	85.54	128.7	.01267	82.85	94.00	.01266	78.99
		10	100	88.2	0.001462	684.0	64.4	0.001509	662.7	47.01	0.001583	631.7
		20	100	176.4	0.005846	171.1	128.7	0.006037	165.6	94.00	0.006330	158.0
			300	176.4	.001949	513.1	128.7	.002012	497.0	94.00	.002110	473.9
	500	20	10	294.1	0.09745	10.26	214.5	0.1006	9.940	156.7	0.1055	9.479
			50	294.1	.01949	51.31	214.5	.02012	49.70	156.7	.02110	47.39
			100	294.1	.009745	102.6	214.5	.01006	99.40	156.7	.01055	94.79
		50	3	735.4	2.031	0.4924	536.2	2.096	0.4771	391.7	2.198	0.4550
			30	735.4	.2031	4.924	536.2	.2096	4.771	391.7	.2198	4.550
			100	735.4	.06092	16.41	536.2	.06289	15.90	391.7	.06594	15.17
Drizzle	100	400	10	1176	7.796	0.1283	857.7	8.050	0.1242	626.7	8.442	0.1185
	300	400	100	3529	2.339	0.4275	2574	2.415	0.4141	1880	2.532	0.3949
			300	3529	.7797	1.283	2574	.8050	1.242	1880	.8440	1.185
	500	400	300	5382	1.299	0.7698	4289	1.342	0.7452	3134	1.407	0.7107
Rain	300	1000	50	8823	29.24	0.03420	6434	30.18	0.03313	4701	31.66	0.03159
			100	8823	14.62	.06840	6434	15.09	.06627	4701	15.83	.06317
			300	8823	4.873	.20520	6434	5.030	.1988	4701	5.277	.1895